



RESEARCH ARTICLE

Design cytotoxicity: The effect of silver nanoparticles stabilized by selected antioxidants on melanoma cells

Anna Barbasz¹  | Agnieszka Czyżowska¹  | Natalia Piergies²  |
Magdalena Oćwieja³ 

¹Institute of Biology, Pedagogical University of Cracow, Krakow, Poland

²Institute of Nuclear Physics, Polish Academy of Sciences, Krakow, Poland

³Jerzy Haber Institute of Catalysis and Surface Chemistry, Polish Academy of Sciences, Krakow, Poland

Correspondence

Anna Barbasz, Institute of Biology, Pedagogical University of Cracow, Podchorążych 2, PL-30-084 Kraków, Poland.

Email: anna.barbasz@up.krakow.pl

Funding information

National Science Centre, Poland, Grant/Award Number: DEC- 2019/03/X/NZ1/00305 - MINIATURA 3

Abstract

Silver nanoparticles (AgNPs) prepared and stabilized by diverse biologically active substances seem to be especially useful in diverse biological and medical applications. The combination of AgNPs with bioactive substances, such as antioxidants, can lead to the development of new systems of desired anticancer properties. In this research, AgNPs were prepared with the use of diverse antioxidant combinations including gallic acid (GA), (–)-epicatechin-3-gallate (EGCG), and caffeine (CAF). The insightful physicochemical characteristic revealed that each type of AgNPs exhibited spherical shape, comparable size distribution and negative surface charge. Surface-enhanced Raman spectroscopy (SERS) delivered the information about the chemistry of AgNP stabilizing layers, which turned out to be a crucial factor tuning toxicity of AgNPs toward murine B16 melanoma cells (B16-F0) and human skin melanoma (COLO 679) cells. EGCGAgNPs were the most cytotoxic among all the investigated AgNPs. They strongly reduced the activity of mitochondria, damaged cell membrane integrity, and penetrated inside the cells causing DNA damage. In turn, the toxicity of GAAgNPs strongly manifested via the induction of oxidative stress in the cells. It was found that CAFGAAgNPs exhibited the lowest toxicity toward the melanoma cells, which proved that a proper combination of antioxidants enable to prepare AgNPs of differentiated toxicity. It was established that human skin melanoma cells were significantly more sensitive to AgNPs than the murine melanoma cells.

KEYWORDS

antioxidants, cytotoxicity, melanoma, silver nanoparticles

1 | INTRODUCTION

For many years, silver nanoparticles (AgNPs) are in the center of interest of scientists dealing with chemistry, material engineering, spectroscopy, and electronic, to name a few. Unusual biocidal properties of AgNPs are the reason of broad range of their biological and medical application (Lee & Jun, 2019). It was documented that AgNPs are able to deactivate diverse types of gram-positive and gram-negative bacteria including also dangerous, pathogenic drug-resistant strains (Zhu et al., 2020). The fungicidal properties of

AgNPs have been confirmed in respect to both mammalian (Panáček et al., 2009) and plant pathogens (Gorczyca et al., 2015). Furthermore, it was shown that AgNPs can act as antiviral agents and exterminate such viruses as hepatitis B (Lu et al., 2008), HIV-1 (Lara et al., 2010), H1N1 influenza A, HPIV3, and even SARS-CoV-2 (Pilaquinga et al., 2021). It is worth mentioning that AgNPs seem to be promising candidates for cancer treatment. Their antiproliferative properties toward, for example, human glioblastoma (U251) (Asharani, Hande, & Valiyaveetil, 2009), breast (MCF-7), lung (A549) (El-Hussein et al., 2015), prostate (PC-3) (He et al., 2016),

and leukemia (HL-60, U-937) (Oćwieja & Barbasz, 2020) cancer cells have been demonstrated.

The possibility of modeling biological activity of AgNPs via the control of their physicochemical properties is the most important advantage in respect to their biological and medical applications. Generally, smaller AgNPs are more toxic than larger ones because they more easily penetrate inside cells (Bae et al., 2011; Kettler et al., 2016). It is also postulated that the enhanced uptake and accumulation of positively charged AgNPs stem from the occurring of attractive electrostatic forces between them and negatively charged cell membranes (El Badawy et al., 2011). The biological activity of AgNPs is also tuned by the stabilizing agent molecules present on their surface. The impact of stabilizing agent molecules on the AgNP toxicity can be indirect, direct, and mixed. In the first case, the molecules adsorbed on AgNP surfaces can influence on the oxidative dissolution and release of silver ions, which are considered as a main factor shaping toxic effect (Kittler et al., 2010). In turn, the direct effects rely on the connection of AgNPs with biologically active stabilizing agents, which leads to the enhancement of biological effects (Fayaz et al., 2010). In some cases, stabilizing agents can stimulate both direct and indirect effects.

Taking these facts into account, the attention of scientist is paid on the preparation of AgNPs with the use of diverse biologically active substances. It is predicted that such approach allows to control AgNP activity at cellular level. Moreover, it is assumed that the involvement of biologically active substances to AgNP preparation will allow to control their selectivity. Among the many reasons of such approach, one can indicate on the fact that it is desired to obtain AgNPs highly toxic for tumor cells and inert for normal cells.

Primary research described in the literature included combined systems formed from AgNPs and antibiotics, which exhibited higher bactericidal properties than these two components applied separately (Ahmad et al., 2019; Hwang et al., 2012). Synergistic effects were also found for the combinations of AgNPs with selected amino acids (Tanvir et al., 2017) or antimicrobial peptides (Ruden et al., 2009). Moreover, the amplified antibacterial activity of AgNPs was observed when they were stabilized by antimicrobial chitosan (Kumar-Krishnan et al., 2015). The application of sodium hexametaphosphate, which is a commonly known permeabilizer of cell membrane, as a AgNP stabilizing agent also amplified the toxicity of nanometric system (Kujda et al., 2015; Oćwieja & Barbasz, 2020).

Bearing in mind the possibility of shaping of bioactive properties of AgNPs, their conjugation with diverse antioxidants seems to be particularly promising for medical purposes. It is worth mentioning that the biological action of AgNPs is related to generation of reactive oxygen species (ROS) which in turn can be reduce by diverse antioxidants.

It is worth emphasizing that in aforementioned studies, the antioxidants were used as additives to previously prepared AgNP suspensions or they were applied after the AgNP treatment. Nevertheless, numerous antioxidants can be used for direct synthesis of AgNPs. For instance, vitamin C is weak reducing agent of silver ions widely applied for preparation of AgNP of tunable sizes (Qin et al., 2010);

3,4,5-trihydroxybenzoic acid known as gallic acid (GA) and its derivative (–)-epicatechin-3-gallate (EGCG) possess similar properties as vitamin C. Besides, these two polyphenols and antioxidants simultaneously exhibit excellent stabilizing properties and well-documented anticancer activity. GA affects several biochemical pathways as a strong antioxidant (Kim et al., 2002), anti-inflammatory agent (Kroes et al., 1992), antimutagenic factor (Gichner, 1987), and anticancer factor (Inoue et al., 1995). In turn, EGCG is a flavonoid from green tea, which suppresses the inflammatory processes that lead to transformation, hyperproliferation, and initiation of carcinogenesis (Thawonsuwan et al., 2010).

1,3,7-trimethylxanthine, which is known as caffeine (CAF), is the next interesting antioxidant of confirmed anticancer activity. CAF is the most frequently ingested pharmacologically active natural alkaloid. CAF has been reported to affect cell cycle function, induce programmed cell death or apoptosis, and perturb key cell cycle regulatory proteins in a concentration-dependent manner (Bode & Dong, 2007). Although it rather does not possess reducing properties toward silver ions, it is possible to use it for AgNP stabilization.

Analysis of available literature reports revealed that despite of aforementioned facts, little is known about toxicity and anticancer activity of AgNPs prepared with the use of these antioxidants. Having regard to these findings, our studies were directed toward development of preparation method of AgNPs with the use of combination of selected antioxidants of confirmed anticancer activity and evaluation of their potential melanoma treatment. Two model types of melanoma cells were selected for the research, namely, mouse melanoma syngeneic model cells (B16-F0) and human malignant melanoma cell line (COLO 679). The research on the lines of the animal is well supported by research on the human lines due to differences in the architecture of the skin and the genesis of melanoma. The main hypothesis of the studies was that the toxicity of AgNPs toward melanoma cells should be dependent on the combination of antioxidants used during the synthesis. It was assumed that antioxidants playing a role of reducing agent of silver ions can appears on the AgNP surfaces in oxidized forms. It was hypothesized that the cell response on the AgNP treatment will be dependent on the structure of their stabilizing agents.

2 | MATERIALS AND METHODS

2.1 | Chemicals

Silver nitrate, 1,3,7-trimethylxanthine (CAF), EGCG, 3,4,5-trihydroxybenzoic acid (GA), ammonia solution (25%), sodium chloride, hydrochloric acid, and sodium hydroxide were purchased from Sigma-Aldrich. These compounds were of analytical grade and were used without further purification. Ultrapure water (Milli-Q water) of conductivity $0.06 \mu\text{S cm}^{-1}$ was obtained using Milli-Q Elix and Simplicity 185 purification system (Millipore SA, Molsheim, France).

2.2 | Synthesis of AgNPs

The AgNPs were prepared in the form of aqueous suspensions applying a chemical reduction of silver ions delivered in the form of silver nitrate by selected antioxidants under alkaline conditions and at ambient temperature. Before the synthesis, all glass vessels and glass elements were cleaned by aqua regia for at least 15 min and thoroughly rinsed with fresh Milli-Q water. An aqueous solution of silver nitrate of concentration of 1 mM was prepared in Milli-Q water, and then it was mixed with 10 ml of aqueous solution of antioxidants keeping a volume ratio of 15:1. CAFGAAgNPs, due to poor reducing properties of CAF, were obtained using antioxidant mixture containing 25 mg of CAF and 4 mg of GA. EGCGGAAgNPs were prepared using a mixture of 5 mg of EGCG and 4 mg of GA. Pure 1-mM solution of EGCG and 2.4-mM solution of GA was used for synthesis of EGCGAgNPs and GAAgNPs, respectively. In order to promote reduction of silver ions and formation of AgNPs, pH of obtained reaction mixtures was increased to the value of 8–9 via addition of 40 μ l of 25% ammonia solution. Newly formed dark brown suspensions of AgNPs were stirred over additional 30 min. Then, each suspension was purified from organic impurities via an ultrafiltration method. For this purpose,

the suspensions were washed with Milli-Q water using a filtration cell Amicon® (model 8400) equipped with membrane made of a regenerated cellulose of nominal molecular weight limit 100 kDa. The purification process was carried out until the conductivity of the effluents stabilized at 20 μ S cm^{-1} and pH attained a value of approximately 5.8–6.1. The stock suspensions were stored in a refrigerator at a temperature of 4°C.

2.3 | Methods applied for characteristics of AgNPs and their suspensions

The density of stock suspensions of AgNPs and obtained effluents was measured with a DMA500 M densitometer (Anton Paar). Knowing the specific density of silver, which is equal to 10.49 g cm^{-3} , and based on the density measurements, the mass concentration of AgNPs in the stock suspensions was determined by applying the procedure described previously (Oćwieja et al., 2017). These values were collected in Table 1. The oxidative dissolution of AgNPs and concentration of released silver ions in the effluents, which were obtained after the separation of AgNPs from ions, were assessed by applying a

TABLE 1 The selected properties of AgNPs and their stock suspensions

Property/conditions [unit]	Sample name			
	CAFGAAgNPs	EGCG AgNPs	EGCGGA AgNPs	GAAgNPs
Compounds used during synthesis	1,3,7-Trimethylxanthine, 3,4,5-trihydroxybenzoic acid	(-)-Epicatechin-3-gallate	(-)-Epicatechin-3-gallate, 3,4,5-trihydroxybenzoic acid	3,4,5-Trihydroxybenzoic acid
Concentration of nanoparticles in the stock suspension [mg L^{-1}]	112	89	128	80
pH of the stock suspension	5.8	6.1	5.9	6.1
Plasmon absorption maximum [nm]	397	402	403	398
Nanoparticle size (diameter) [nm] form TEM micrographs	12 \pm 4	14 \pm 6	13 \pm 4	10 \pm 3
Diffusion coefficient [$\times 10^{-7} \text{ cm}^2 \text{ s}^{-1}$] $T = 37^\circ\text{C}$, pH 7.4, $I = 10^{-2} \text{ M}$ determined from DLS technique	5.37	4.96	4.96	5.37
Hydrodynamic diameter [nm] calculated from diffusion coefficient $T = 37^\circ\text{C}$, pH 7.4, $I = 10^{-2} \text{ M}$	12 \pm 3	13 \pm 5	13 \pm 2	12 \pm 2
Polydispersity index (Pdl) determined by DLS	0.25	0.38	0.15	0.16
Electrophoretic mobility [$(\mu\text{mcm}) (\text{Vs})^{-1}$] determined for $T = 37^\circ\text{C}$, pH 7.4, $I = 10^{-2} \text{ M}$	-3.64 \pm 0.04	-4.37 \pm 0.04	-4.64 \pm 0.04	-3.59 \pm 0.04
Zeta potential [mV] determined for determined for $T = 37^\circ\text{C}$, pH 7.4, $I = 10^{-2} \text{ M}$	-58 \pm 3	-68 \pm 4	-72 \pm 3	-56 \pm 3

pH/ionometer Seven Compact™ (Mettler Toledo) equipped with silver/sulfide electrode perfectION™.

The optical properties of AgNPs were studied, with extinction spectra of their suspensions recorded by a UV-2600 spectrometer (Shimadzu). For this purpose, the AgNPs were dispersed in an aqueous suspensions of controlled pH, ionic strength, and temperature, as well as in an RPMI 1640 and DMEM medium supplemented by 10% fetal bovine serum (FBS) and 0.01% penicillin–streptomycin.

The morphology and size distribution of AgNPs were evaluated using micrographs recorded using a JEOL JSM-7500F electron microscope working in the transmission mode (transmission electron microscopy [TEM]). The analysis of micrographs was conducted in MultiScan software (Computer scanning system). The histograms were obtained based on the analysis of 1000 nanoparticles.

The stability of AgNPs dispersed in suspensions of controlled pH, ionic strength, and temperature of 37°C was studied conducting measurements of their diffusion coefficients (D) and electrophoretic mobility (μ_e) by Zetasizer Nano ZS (Malvern).

The chemical composition of AgNP stabilizing layers was studied through the use of surface-enhanced Raman spectroscopy (SERS). The SERS spectra were recorded using a Renishaw InVia Raman spectrometer equipped with a 632.8-nm laser line and a CCD detector thermoelectrically cooled to -70°C . A dry Leica N PLAN EPI (20 \times , NA 0.4) objective was applied for measurements. The output laser power was approximately 2 mW. For each sample, one scan with an integration time of 30 s and a resolution of approximately 1 cm^{-1} was collected. The spectrometer was calibrated using the Raman scattering line produced by an internal silicon plate. The measurements were performed for the AgNP suspension of regulated ionic strength. For this purpose, an appropriate amount of 1-M sodium chloride solution was added to obtain the suspension of ionic strength of 100 mM. Then, the suspension was dropped onto a platinum holder. A laser spot was focused inside the drop and a measurement was taken. Additionally, the Raman spectra of CAF, EGCG, and GA powders were also recorded and analyzed.

The purity of AgNP suspensions was also assessed considering the content of endotoxin contamination. The ToxinSensor™ Chromogenic LAL Endotoxin Assay Kit (Genescript, Piscataway, NJ, USA) was introduced to the investigation to determine the content of lipopolysaccharide (LPS) contaminations. The AgNP dispersions in the culture media of mass concentration of 25 mg L^{-1} were applied in these studies. The detection of endotoxins was conducted according to the manufacturer's instructions in the supernatants obtained after a centrifugation of the suspensions at $10,000\times g$ for 15 min.

2.4 | Cell lines

Murine B16 melanoma cells (B16-F0) and human skin melanoma (COLO 679) cells were supplied by ECACC. B16-F0 cells were grown in DMEM supplemented medium and COLO 679 cells were grown in RPMI 1640 medium, both with 10% fetal bovine serum (FBS) and 0.01% penicillin–streptomycin at 37°C in a humidified atmosphere of

5% CO_2 . The culture medium, FBS, and antibiotics were purchased from PAN-Biotech GmbH.

2.5 | Cell viability

To evaluate cell proliferation, XTT assay kit (Abcam; ab232856) was used according to the manufacturer's instructions. The cells were cultured in 96-well plates in an amount of 10×10^3 cells per well in a volume of 0.2 ml/well. After a 24-h exposure of cells to the AgNPs (or pure organic reagents), the medium was exchanged and a reaction mixture was added for 2 h. Absorbance of supernatant was read on a microplate reader (Epoch BioTek Instruments microplate reader) at 450 nm. Based on the results of the cell survival presented in this paper, the values of the median lethal dose (LD_{50} median lethal dose) for cells were calculated using Behrens' method (Zbinden & Flury-Roversi, 1981) with the following assumptions: the number of cells per measurement point is constant, the absorbance determined in the XTT method is correlated with the number of live cells (if the cell is experiencing a higher dose, it has survived all lower doses; if the cell dies at the lower dose, it would die at all higher doses). Then, the percentage mortality was calculated for each dose of nanoparticles and LD_{50} values were obtained from appropriate graphs.

2.6 | Cell membrane damage and LDH release

Lactate dehydrogenase leakage (LDH assay) was used for determination of the membrane stability of the cells after the AgNPs treatment. The supernatant of cells (100 μl), after centrifugation, was added to a mixture containing 500 μl of 0.75-mM sodium pyruvate and 10 μl of 140- μM NADH. Such mixtures were incubated at temperature of 37°C over 30 min. Afterwards, 0.5 ml 1 mM solution of 2,4-dinitrophenylhydrazine in 1-M HCl was added to each of the mixtures. After 1 h of addition, the absorbance of formed hydrazone was measured at 450 nm using the microplate reader Epoch (BioTek Instruments).

2.7 | Membrane lipid peroxidation

Membrane lipid peroxidation was assessed spectrophotometrically measuring absorbance of thiobarbituric acid and malodialdehyde (MDA) complex at 532 nm. The cells were cultured in 24-well plates in an amount of 50×10^3 cells per well in a volume of 0.5 ml per well. Cells were treated with selected factors, adjusted to a final volume of suspension equal to 0.5 ml and kept for 24 h. To obtain supernatants, 0.5 ml of 0.5% trichloroacetic acid (TCA) was added. Then, the mixtures were vortexed for 1 min and then lysed over 5 min using ultrasonic bath (15 kHz). The samples were centrifuged (10 min, $10,000\times g$) and finally added to 1.25 ml of solution of 20% TCA and 0.5% TBA. After 30 min of heating at 100°C, the samples were cooled

to ambient temperature and characterized. MDA concentration was determined spectrophotometrically at $\lambda = 532$ nm at room temperature, corrected for nonspecific background by subtracting the absorbance at $\lambda = 600$ nm. The MDA concentration was calculated using the molar extinction coefficient of $155 \text{ mM}^{-1} \text{ cm}^{-1}$.

2.8 | Nitric oxide production

The cells were cultured in 24-well plates in an amount of 50×10^3 cells per well in a volume of 0.5 ml per well. The cells were treated with selected factors, adjusted to a final volume of suspension equal to 0.5 ml and kept for 24 h. After treatment, the supernatants were collected, centrifuged ($1000 \times g$, 5 min) and stored at -20°C . Nitric oxide (NO) production from treated cells was quantified spectrophotometrically using the Griess reagent (modified) (Sigma). The absorbance was measured at 540 nm, and the nitrite concentration was determined using a calibration curve.

2.9 | The total cell resistance to oxidation

The total cell resistance to oxidation (TRO) before and after treatment with the AgNPs of concentration ranged between 6.25 and 25 mg L^{-1} was tested by the modified spectrophotometric 2,2-diphenyl-1-picrylhydrazyl radical scavenging (DPPH) assay (Blois, 1958). The cells were cultured in 24-well plates in an amount of 50×10^3 cells per well in a volume of 0.5 ml per well. The pellets of cells, after centrifugation, were mixed with 0.2 ml of absolute methanol. The samples were vortexed for 1 min and then centrifuged (10 min , $10,000 \times g$). Next, 0.1 ml of supernatant and 0.2 ml of 0.125-mM DPPH on a 96-well plate were incubated for 30 min at room temperature in the dark. The absorbance of samples was measured at 517 nm using a microplate reader. Methanol was used as a control sample. TRO of human cells representing ability to counteract oxidation reaction, was calculated from the formula:

$$\% \text{inhibition} = 100 \frac{A_{\text{control}} - A_{\text{sample}}}{A_{\text{control}}}$$

2.10 | Generation of ROS

Free radicals and other ROS were detected using a Cellular ROS/Superoxide Detection Assay Kit (Abcam, ab139476). In a 0.2-ml suspension, 10×10^3 cells/ml were incubated with the AgNPs of concentration of 25 mg L^{-1} and then with a ROS/Superoxide Detection Mix for 30 min at 37°C . The positive control was incubated with 0.2 mmol/L pyocyanine. Then, the fluorescence intensities were measured at an emission wavelength of 520 nm (green) and 610 nm (orange; excitation wavelengths: 485 and 550 nm), respectively, using a microplate reader.

2.11 | Evaluation of DNA damage

The cell culture containing 2×10^6 cells was collected from culture flasks. Then, after the cell exposure to the AgNPs of concentration equal to 25 mg L^{-1} , the samples were centrifuged. DNA from the cells was extracted using a DNA isolation kit from animal tissues and cell lines (Extractme, EM03-050). Then, the DNA damage was estimated using Abcam DNA Damage AP Sites Assay Kit (Abcam, ab65353) standard protocol. The relative number of AP sites was estimated by comparison of the absorbances (450 nm) value from control cells (not treated).

2.12 | Evaluation of nuclei disruption

In order to investigate the fragmentation of nuclei, the 10×10^3 cells in a 0.2-ml suspension were treated with the AgNPs of concentration 25 mg L^{-1} for 24 h and then stained with $1 \mu\text{g ml}^{-1}$ 4',6-diamidino-2-phenylindole (DAPI) (DAPI-DNA complex $\text{Ex} = 364 \text{ nm}$; $\text{Em} = 454 \text{ nm}$). The morphology of a nucleus was observed using a Canon EOS 60D camera and a Delta IB-10 optical microscope set with a U filter (420 nm).

2.13 | The cell imaging with TEM

The cells were cultured in culture flasks in an amount of 2×10^6 cells per flask. After 24 h of incubation with the AgNPs of concentration of 25 mg L^{-1} , the cells were washed with PBS and then detached from the support using a 2-mM EDTA in PBS solution. After centrifugation, the cells were suspended in complete medium. Then, the cells were fixed in 2.5% glutaraldehyde in 0.1-M cacodylate buffer, pH 7.3, at 10°C (Polysciences, Warrington, PA, USA) for 24 h. After the washing procedure, they were postfixed in 1% osmium tetroxide in cacodylate buffer for 1 h. Then, the cells were washed in cacodylate buffer again and dehydrated in 50%, 70%, 96%, and 100% ethanol. At the end, they were treated with propylene oxide twice for 5 min and embedded in a Poly/Bed 812 (Polysciences). After polymerization, 70-nm-thick sections were cut on a Leica UC7 ultramicrotome, collected on copper Formvar-coated single-slot grids, and contrasted with uranyl acetate and lead citrate. Sections were viewed and photographed using a JEOL (Tokyo, Japan) 2100HT electron microscope.

2.14 | Statistical analysis

Each AgNP concentration was investigated in five independent replicates and averaged, which allowed the determination of the standard deviation value. Significant differences compared with the controls were estimated based on the SAS ANOVA procedure. The statistical analysis of the results obtained from each of the above-mentioned biochemical assays was carried out using the Duncan multirange test, assuming $p < 0.05$ using the PC SAS 8.0 software (SAS Institute).

3 | RESULTS

3.1 | Characteristics of AgNPs

Four types of AgNPs were obtained in a chemical reduction of silver ions by selected low molar mass organic compounds belonging to antioxidants (Table 1). The purification process allowed obtaining of AgNP suspensions of controlled pH, ionic strength, and low content of organic contaminations. It was established that mass concentration of AgNPs in the stock suspensions ranged between 80 and 130 mg L⁻¹ (Table 1). Silver ions were not detected in the effluents obtained from freshly cleaned suspensions. The effluents collected from the suspensions after 30 days of storage in the refrigerator were free from silver ions, which indicates that the AgNPs obtained using the antioxidants were susceptible to oxidative dissolution.

Recorded extinction spectra revealed that the appearance of the maximum absorption band is correlated with the composition of antioxidants used for AgNP synthesis (Figure S1). The maximum absorption bands of CAFGAAgNPs and GAAgNPs occurred at 397 and 398 nm. In the case of AgNPs prepared using EGCG, absorption maxima were detected at wavelength of 402 and 403 nm (Table 1). The extinction spectra were also measured for the AgNPs dispersed in the culture media (Figures S2 and S3). These studies revealed that the absorption maxima were bathochromic shifted in comparison with these ones recorded in the diluted aqueous suspensions. Because the appearance and intensity of the bands recorded in the culture media were not changed over time, it was established that observed differences in the spectra result from the interactions occurring between FBS and antibiotics, which influence on a localized surface plasmon resonance (LSPR). Having regard to the invariability of spectra over time, the aggregation of AgNPs in the culture media were excluded.

TEM micrographs revealed that the AgNPs were spherical nanostructures of comparable size distribution and an average size (Figure S4). It was established that GAAgNPs exhibited the smallest average size, which was equal to 10 ± 3 nm. In turn, EGCGAgNPs were characterized by the largest average size, which attained a value of 14 ± 4 nm (Table 1).

The physicochemical properties of AgNPs were also evaluated in the suspensions of controlled ionic strength and pH with the use of dynamic light scattering (DLS) and electrophoretic light scattering (ELS). The determination of the values of diffusion coefficient (*D*) and electrophoretic mobility (μ_e) of AgNPs was carried out at temperature of 37°C, which is typical for biological tests. The results of measurements were used to calculate the hydrodynamic diameter (d_h) and the zeta potential (ζ) of the AgNPs based on the Stokes–Einstein equation and Henry's model, respectively (Oćwieja & Adamczyk, 2014). The data achieved at ionic strength of 10⁻² M, pH 7.4, and temperature of 37°C were collected in Table 1. Analyzing these values, one can notice that the average size evaluated based on TEM micrographs remained in good agreement with the hydrodynamic diameters of AgNPs. The dependencies of AgNP hydrodynamic diameters on ionic strength and pH were presented in Figure S5. Generally, it was established that at pH of 6.1, the AgNPs aggregated for ionic strength higher than

3 × 10⁻² M. At lower ionic strengths, the AgNPs were stable in the entire investigated range of pH, namely, from 2 to 10. Independently of the composition of antioxidants used during the preparation, the AgNPs were negatively charged. The zeta potential attained highly negative values especially in the case of EGCGAgNPs and EGCGG AAgNPs (Table 1). Regardless of antioxidants applied for the preparation, the zeta potential of AgNPs was negative for broad range of ionic strength and pH (Figure S6). It was established that the AgNPs did not possess an isoelectric point in the pH range from 2 to 10. The zeta potential of EGCGGAAgNPs was the most negative among all investigated nanoparticles. In turn, GAAgNPs were characterized by the least negative zeta potential for each value of pH (Figure S6). These observations unambiguously indicate that the composition of antioxidants used for the AgNP synthesis affects their electrokinetic properties. It is worth mentioning that the hydrodynamic diameter and zeta potential of AgNPs dispersed in culture media were not investigated due to the disruption of DLS and ELS measurements by a high excess of FBS in comparison with mass concentration of nanoparticles.

In order to characterize the AgNPs more precisely, the chemical composition of their stabilizing layers was assessed using SERS. Additionally, the spectra of pure antioxidants used for the synthesis of AgNPs were recorded using classical Raman spectroscopy (RS). Recorded RS and SERS spectra were presented in Figures S7 and S8. In Figure S7, one can see the RS spectra of GA and CAF together with the SERS spectrum of CAFGAAgNPs. The compiled spectral data demonstrates that the characteristic RS bands attributed to the specific functional groups of the stabilizing agents are observable in the SERS spectrum. This confirms their presence on CAFGAAgNPs surface. Chen et al. (2010) described how CAF anchor to the borohydride-reduced AgNPs. It was suggested that this molecule adopts parallel orientation on the AgNPs and C–N bond interacts with the nanoparticles. However, this adsorption pattern differs for the citrate-stabilized AgNPs. Pavel et al. (2003) proved that CAF adsorbs on these AgNPs through a C=O bond with a perpendicular orientation of the whole molecule to the metal surface. The relative intensities and positions of the SERS bands characteristic for CAF on CAFGAAgNPs illustrate some differences in the adsorption orientation of this molecule in comparison with the above-mentioned AgNP surfaces. Briefly, the RS bands at 1600, 1408, 1328, 1240, 1020, 740, and 555 cm⁻¹ are assigned to the C=C symmetric stretching/C–N symmetric stretching/CH₃ symmetric bending ($\nu_s(\text{C}=\text{C})/\nu_s(\text{CN})/\rho_{bs}(\text{CH}_3)$), the C–N symmetric stretching ($\nu_s(\text{CN})$), the imidazole trigonal stretching ($\nu(\phi_{\text{imid}})$), the C–N stretching ($\nu(\text{CN})$), the N–CH₃ asymmetric stretching ($\nu_{as}(\text{N}-\text{CH}_3)$), the O=C–C deformation ($\delta(\text{O}=\text{C}-\text{C})$), and the O=C–C deformation/pyridine ring breathing vibrations ($\delta(\text{O}=\text{C}-\text{C}/\text{Pyr}(\text{breath}))$), respectively (Chen et al., 2010; Kang et al., 2011; Pavel et al., 2003). In the SERS spectrum, these bands are observed at 1608, 1398, 1329, 1253, 1002, 746, and 556 cm⁻¹, respectively. On the one hand, the weak intensity of 1328, 740, and 555 cm⁻¹ spectral features suggests that the planes of pyridine and imidazole trigonal rings are parallel to the NP surface (Chen et al., 2010). On the other hand, the strong intensity of the

1608-cm⁻¹ band together with the visible medium intensity of the 1398- and 1329-cm⁻¹ bands indicate the rather tilted orientation of CAF molecule on the metal surface. This statement is also supported by the appearance of the spectral feature at 1132-cm⁻¹ characteristic for the C-N symmetric stretching modes ($\nu_s(\text{CN})$). Also some SERS bands attributed to GA are noticeable for CAFGAAgNPs. In the RS spectrum, these bands occur at 1530 cm⁻¹ (the aromatic C-C stretching modes; $\nu(\text{CC})_\phi$), 1264 cm⁻¹ (the out-of-plane C=O stretching modes; $\nu_{o,p}(\text{C=O})$), 1216 cm⁻¹ (the deformation O-H modes; $\delta(\text{OH})$), 801 cm⁻¹ (the CH₃ bending modes; $\rho_b(\text{CH}_3)$), 774 cm⁻¹ (the C-C stretching/C-O deformation modes; $\nu(\text{CC})_\phi/\delta(\text{CO})$), 700 cm⁻¹ (the C-O torsion modes; $\gamma(\text{CO})$) (Alvarez-Ros et al., 2001, 2003; Garrido et al., 2016). The corresponding SERS spectral features are observable at 1527, 1267, 1216, 801, 768, and 709 cm⁻¹, accordingly. Previously published results by Alvarez-Ros et al. (2001, 2003) suggest that GA can be present on the AgNPs as a mixture of aliphatic and aromatic moieties. However, the spectral features occurring in the SERS spectrum exclude the possible ring opening of the GA molecule on the CAFGAAgNPs surface due to the fact that no band characteristics for the aliphatic C-H bonds, especially in the high spectral range (3000–2700 cm⁻¹; not shown), are visible. The strong enhancement of the $\nu(\text{CC})_\phi$ and $\delta(\text{OH})$ SERS bands in comparison with the corresponding RS bands indicates the presence of the aromatic moiety of GA on the metal surface and their strong interaction with the CAFGAAgNPs. These spectral patterns coupled with the occurrence of the band due to the $\nu_{o,p}(\text{C=O})$ shows the tilted orientation of the GA molecule on the AgNP surface.

Conversely, GA adopts different forms as the stabilizing layer of GAAgNPs. Previously considered results (Barbasz et al., 2021) proved that GA stabilizes GAAgNPs in two forms, namely, as hydroxylated aliphatic and phenolic moieties. Such a statement was based on the appearance of the strong intensity bands at 2927 cm⁻¹ assigned to the aliphatic C-H stretching mode ($\nu(\text{CH})$) and at the same time at 1592-cm⁻¹ characteristic for the aromatic C=C stretching vibrations ($\nu(\text{C=C})_\phi$) in the SERS spectrum of GAAgNPs (Barbasz et al., 2021). As it was mentioned above, such possible coexistence of two forms of GA on the AgNPs has been already proved (Alvarez-Ros et al., 2001, 2003).

The SERS spectra of EGCGAgNPs and EGCGGAAgNPs showed in Figure S8 represent similar spectral features as a result of the presence of the EGCG molecules on the both AgNP surfaces. Because it is known that EGCG is a GA ester, the RS and SERS spectra of catechins and GA can also be used to identify EGCG by vibrational spectroscopy (Alvarez-Ros et al., 2001, 2003; Garrido et al., 2016; Huang & Chen, 2018; Xia et al., 2020). Without a doubt, the SERS bands observed at 1619, 1341, and 1044 cm⁻¹ for EGCGAgNPs and at 1613, 1344, and 1040 cm⁻¹ for EGCGGAAgNPs prove the occurrence of EGCG on the both AgNP surfaces. These bands are assigned to the D ring breathing, the C-O stretching ($\nu(\text{CO})$), and the OH bending vibrations ($\rho_b(\text{OH})$) and are visible in the RS spectrum of EGCG at 1629, 1346, and 1034 cm⁻¹, respectively. The strong enhancement of the D ring breathing bands in the discussed SERS spectra together with the appearance of the bands at 1509 and 1518 cm⁻¹ characteristic for the ring stretching modes (not observed in the RS spectrum of EGCG)

indicates that the aromatic moieties of EGCG interact with both types of AgNPs. Also, the OH bonds appear to be involved in the anchoring of the EGCG molecules to the AgNP surfaces. The strong enhancement of the SERS band at 1044 cm⁻¹ in the spectrum of EGCGAgNPs in comparison with the RS spectrum of the nonadsorbed EGCG corresponds to the interaction between OH bonds and the AgNPs. Such OH/AgNPs interaction appearing for catechin has been already described (Huang & Chen, 2018). However, the intensity of the considered band decreases significantly in the SERS spectrum of EGCGGAAgNPs. This spectral pattern can have a twofold explanation. First, the observed changes in the intensity of the 1040-cm⁻¹ band may indicate reorientation of the EGCG molecule on the EGCGGAAgNPs in such direction that the OH bond is not close to the metal surface. Second, this may be an evidence of the EGCG oxidation on the metal. It has been proved that catechin derivatives, including EGCG, undergo oxidation very easily in neutral and alkaline pH conditions (Hong et al., 2002; Peter et al., 2020). Due to the fact that during the synthesis procedure (please see Section 2.2) the high pH was applied for promoting reduction of silver ions, the oxidized form of EGCG on the NP surfaces is expected. Indeed, the presence of the bands at 1264 and 1271 cm⁻¹ in the SERS spectra of EGCGAgNPs and EGCGGAAgNPs, respectively, (not observed in the RS spectrum of the non-adsorbed EGCG), which are attributed to the $\nu_{o,p}(\text{C=O})$, supports the possible oxidation that occurs on the both types of AgNPs. Also, in the SERS spectrum of EGCGGAAgNPs (Figure S8), bands manifesting the presence of GA on the AgNP surface are noticeable. These bands appear at 1518 ($\nu(\text{CC})_\phi$) and 1220 cm⁻¹ ($\delta(\text{OH})$). Moreover, the C=O bond vibrations of GA have contribution to the band at 1271 cm⁻¹. Similarly, as it was identified for CAFGAAgNPs, GA adsorbs on the EGCGGAAgNPs as the phenolic moiety.

At the last stage of physicochemical characteristics of AgNPs, their purity toward the endotoxin content was carefully determined. The endotoxin content was equal to 0.104 ± 0.013 , 0.072 ± 0.011 , 0.091 ± 0.025 , and 0.091 ± 0.025 EU ml⁻¹ for CAFGAAgNPs, EGCGAgNP, EGCGGAAgNPs, and GAAgNPs, respectively

3.2 | Impact of antioxidants and AgNPs on cell viability

XTT assay was applied to evaluate the changes in the mitochondrial activity of the cells after their exposure to the antioxidants and obtained AgNPs. In preliminary experiments, the dose-dependent effect of individual antioxidants on the cell survival was determined (Figure S9). CAF showed the lowest toxicity toward both melanoma cell lines. A decrease of cell viability by 20% compared with the control at the CAF concentration of 500 mg L⁻¹ was found, in terms of statistical differences. In turn, the cell treatment by CAF solution of concentration equal to 25 mg L⁻¹ reduced the cell viability only to 95%. For comparison, EGCG solution of concentration 25 mg L⁻¹ caused that the cell viability to decrease to 95% and 85% in the case of B16-F0 and COLO679, respectively. GA was the most cytotoxic among the tested antioxidants. At a GA concentration of 25 mg L⁻¹,

the viability of B16-F0 and COLO 679 cells decreased by 50% and 20%, respectively, in comparison with the control. On the basis of the obtained results, LD₅₀ was determined for the antioxidants alone, based on the Behrens method (Table S2). Among the tested antioxidants, CAF shows the lowest cytotoxicity in terms of melanoma cells (LD₅₀ of 600 mg L⁻¹/1 × 10⁶ cells). GA is the most cytotoxic with respect to both cell lines (LD₅₀ of 10 mg L⁻¹/1 × 10⁶ cells). The cell response to EGCG treatment is the most diverse. Human cells are less sensitive to their treatment with EGCG than mouse cells.

The results of studies obtained for B16-F0 and COLO 679 cells treated by the AgNPs were shown in Figure 1A,B, respectively. Analyzing the results, one can notice that the cell lines differ in survival after the exposure to diverse doses of AgNPs. The human COLO 679 line was more sensitive to the AgNP treatment compared with the mouse B16-F0 cell line. This dependence is the most noticeable for the treatment with the highest concentration of AgNPs.

In turn, the viability of B16-F0 cells decreased on average by about 28% compared with the control sample after the treatment

with all types of AgNPs at concentration of 25 mg L⁻¹. One can notice that EGCGAgNPs turned out to be the most toxic for human COLO679 cell line. The highest concentration of these AgNPs killed all COLO679 cells (Figure 1B). GAAgNPs were the least toxic for the human cell line, whereas the effects induced by CAFGAAgNPs and EGCGAgNPs were rather indirect. In the case of both lines, the concentrations of the AgNPs below 6.25 mg L⁻¹ did not affect the statistical difference of the result against the control in terms of statistical differences.

The results of cell viability allowed the determination of the LD₅₀ values. Data presented in Table 2 show that LD₅₀ values for the B16-F0 cells were much higher than for COLO 679 cells. Interestingly, it was found that that LD₅₀ determined for EGCGAgNPs was equal to 57.5 and 10.2 mg L⁻¹ in the case of B16-F0 and COLO 679 cells, respectively. Hence, these AgNPs turned out to be the most harmful for the human line and the least toxic for the mouse cell line.

Complementary research was conducted with the use of negatively charged citrate-stabilized AgNPs (hereafter marked as

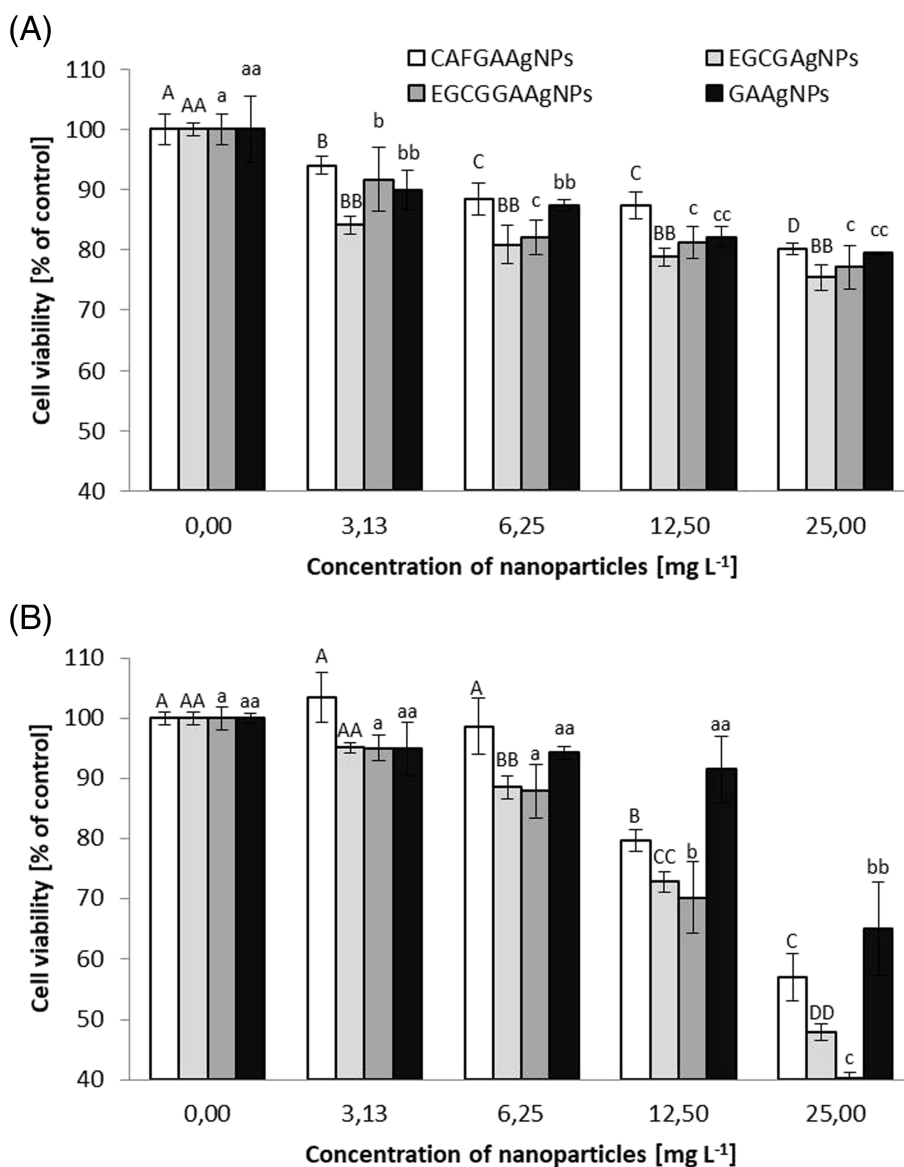


FIGURE 1 The effect of AgNPs on viability of (A) B16-F0 and (B) COLO 679 cells. The viability of cell lines was determined after 24 h of AgNP treatment using XTT assay. Values represent mean ± SD of three to five independent experiments. Different letters indicate significant differences ($p \leq 0.05$) between the tested systems in compared to controls

	LD ₅₀ (mg L ⁻¹ /1 × 10 ⁶ cells)			
	CAFGAAgNPs	EGCGAgNPs	EGCGGAAgNPs	GAAgNPs
B16-F0	50.1 ± 2.5	57.5 ± 2.9	40.9 ± 2.0	42.8 ± 2.1
COLO679	18.7 ± 0.9	10.2 ± 0.5	14.3 ± 0.7	23.1 ± 1.1

TABLE 2 The effect of treatment (24-h incubation) of melanoma cell lines by the AgNPs on the average lethal dose (LD₅₀)

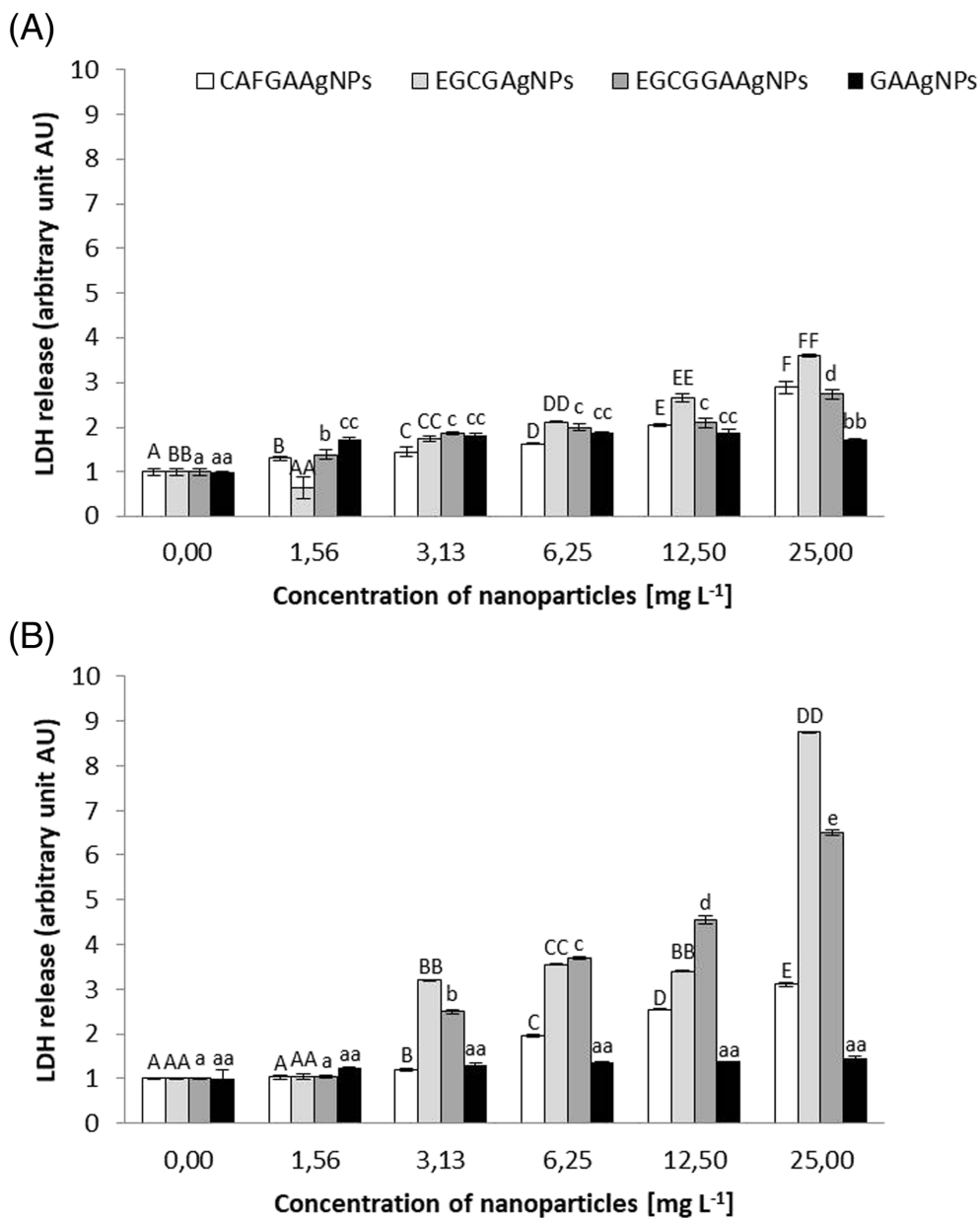


FIGURE 2 Cell membrane damage indicated via LDH release after the 24 h treatment of (A) B16-F0 and (B) COLO 679 with AgNPs. Values represent mean ± SD of three to five independent experiments. Different letters indicate significant differences ($p \leq 0.05$) between the tested systems in compared to controls

SBTCaAgNPs) of an average size equal to 14 ± 5 nm, which were prepared without any antioxidants (Barbasz, Oćwieja, & Roman, 2017). The melanoma cell viability after the SBTCaAgNP treatment was presented in Figure S10. Interestingly, B16-F0 cells were insensitive to SBTCaAgNP exposure in the investigated concentration range. At SBTCaAgNP concentration equal to 25 mg L^{-1} , the B16-F0 cell viability maintained at the level 82%. Based on these results, one can state that the toxicity of SBTCaAgNPs and antioxidant-stabilized AgNPs toward murine melanoma cells was analogous. The viability of COLO

679 cells was strongly dependent on the SBTCaAgNP concentration (Figure S10). The increase of SBTCaAgNP concentration from 6.25 to 25 mg L^{-1} caused the drop of viability of COLO 679 cells from 82% to 35%. The LD₅₀ values for SBTCaAgNP (Table S2) indicate a lower value of this parameter for uncoated nanoparticles than for antioxidant-stabilized silver nanoparticles (the average LD₅₀ value for B16-F0 was 47.8 and for COLO 679 was 16.6).

In the next part of studies, the attention was focused on the determination of cell membrane destruction occurring as the result of

AgNP treatment. LDH assay was introduced to evaluate the AgNP-induced destruction of the melanoma cell membranes. Obtained data were presented in Figure 2 as dependencies of LDH release on the AgNP concentration. The LDH release was dose dependent and the increase of the AgNP concentration enhanced secretion of this membrane damage mediator. Analyzing the results gathered for B16-F0, one can notice that for a given AgNP concentration, the LDH release was insignificantly dependent on the type of AgNP. Nevertheless, EGCGAgNPs seemed to be the most destructive for these cells as well as for the human line. Along with the increase in the concentration of AgNPs, a threefold increase in LDH activity in the culture medium for mouse cells and significantly higher for human cells was observed. On the other hand, COLO 679 cells were considerably more prone to the AgNP action. The results showing damage to the cell membranes correlate with the results of the mitochondrial activity test (Figure 1). The detection of malondialdehyde (MDA) was used to determine the level of peroxidation of membrane lipids as the consequence of the AgNP treatment. The results of AgNP concentration-dependent secretion of MDA were presented in Figure 3A,B. It was found that at the lower concentration of AgNPs, their impact on MDA secretion was rather negligible. The highest MDA content was determined for the AgNP concentration of 25 mg L⁻¹. These results revealed also that COLO 679 cells were more prone to peroxidation of membrane lipids than

B16-F0, especially after the treatment with EGCGAgNP and GAAgNPs. It was also observed that CAFGAAgNPs causes the smallest increase in lipid peroxidation in B16-F0 cells. In COLO 679 cells, the smallest effect was observed after treatment of CAFGAAgNPs and EGCGGAAgNPs.

The next stage of the research was to check whether the AgNPs are immunogenic. For this purpose, the concentration of the universal inflammatory mediator NO was determined. Analyzing the data shown in Figure 3C,D, one can observe that the production of NO was the most stimulated for both cell lines by CAFGAAgNPs and EGCGAgNPs. For example, the EGCGAgNPs at concentration of 25 mg L⁻¹ induced a fivefold increase in the NO concentration in comparison with the control groups of both cell lines. In turn, the GAAgNP treatment of the same concentration led to the twofold to threefold enhanced NO secretion in respect to the control.

DPPH assay was applied in order to evaluate the total cell resistant to oxidation (TRO). The results of studies expressed as a reduction of DPPH level in the AgNP treated cells in comparison with the control sample involved the untreated cells were shown in Figure S11. It was observed that the cell exposure to AgNPs caused a decrease in their resistance to oxidation, which was significantly dependent on the types of AgNPs. The strongest effect was noted for COLO 679 cells treated by CAFGAAgNPs of the highest

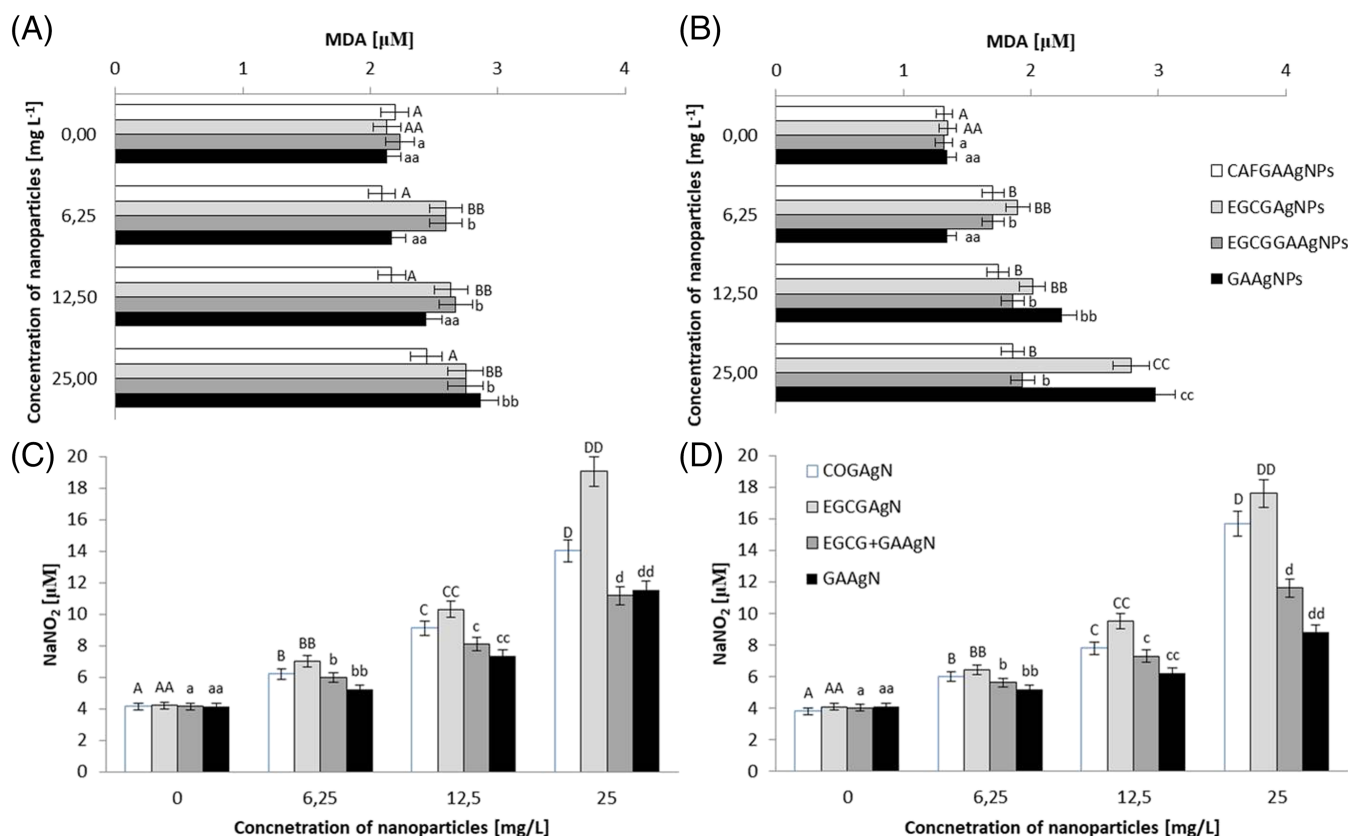


FIGURE 3 Effects of AgNPs on cell membrane integrity express by the content of malondialdehyde (MDA) in (A) B16-F0 and (B) COLO 679 cells after 24 h treatment with AgNPs of different concentrations. Level of NO secreted by (C) B16-F0 and (D) COLO 679 after the contact with the AgNPs was quantified spectrophotometrically using the Griess reagent. Values represent mean \pm SD of three to five independent experiments. Different letters indicate significant differences ($p \leq 0.05$) between the tested systems in compared to controls

concentration. In the case of B16-679 cells, the TRO was decreased by 50% in comparison with the control group after the treatment by the AgNPs of concentration 25 mg L^{-1} . The effect was independent on the types of AgNP coating.

The generation of ROS as the result of the exposure to AgNPs of concentration of 25 mg L^{-1} was demonstrated in Figure 4A. The presence of AgNPs increased the total amount of ROS in both cell lines. The greatest ROS increase was observed after the treatment with EGCGAgNPs and GAAgNPs. In turn, the CAFGAAgNPs induced the lowest ROS generation in both melanoma cell lines.

Because a major consequence of increased ROS production is DNA damage, thus this process was assessed by determining the number of AP sites in the cells after the treatment with AgNPs. The results of studies shown in Figure 4B revealed that the presence of AgNPs of concentration of 25 mg L^{-1} caused a significant increase of number of AP sites in comparison with the control group. For example, the fivefold and sixfold increase in the number of AP sites was detected in COLO 679 cells after the exposure to CAFGAAgNPs and

EGCGGAAgNPs, respectively. Similarly, significantly enhanced DNA damage in B16-F0 cells was determined after the treatment with EGCGAgNPs and EGCGGAAgNPs.

The morphological changes of the cells treated with the AgNPs were evaluated based on the results obtained using DAPI assay combined with optical microscope imaging. Additionally, the cell visualization with the use of TEM was applied for more precise research. The microscope images obtained after DAPI staining were presented in Figure S12. Analyzing these images, one can observe that after the AgNP treatment, the number of damaged cells significantly increased compared with the control group. Additionally, the presence of more segmented cell nuclei indicated that their nucleus was significantly damaged.

The visualization of the cells using TEM revealed additional changes in their ultrastructure after the treatment with AgNPs. The extremely complex structure of the cells was altered in the presence of the AgNPs, which is visible in Figure 5. Compared with the control, more mitochondria with possibly damaged inner mitochondrial

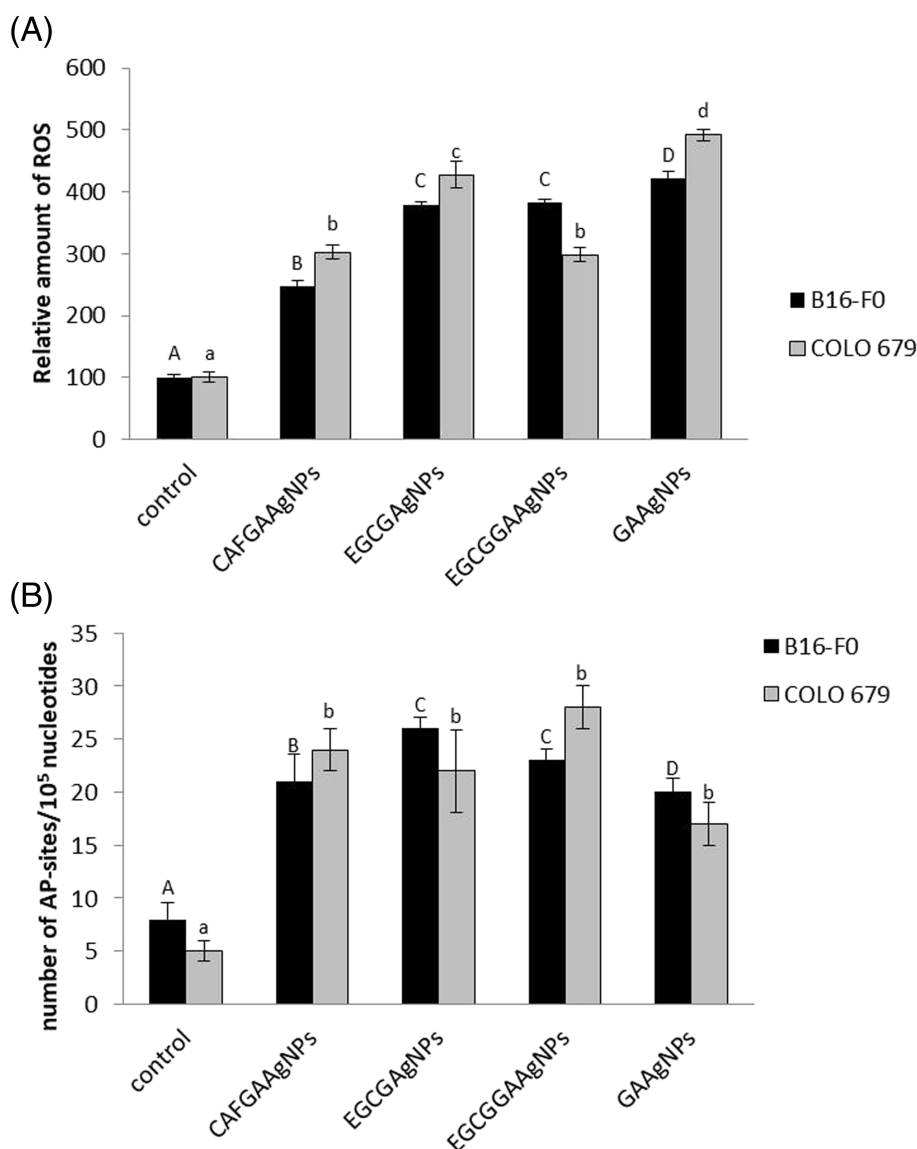


FIGURE 4 (A) Relative increase of the intracellular concentration of ROS in melanoma cells after 24 h of treatment with the AgNPs of concentration of 25 mg L^{-1} . The ROS level was calculated as mean \pm SD with respect to untreated control set to 100%. (B) Levels of AP-sites in the DNA of the cells after their treatment with the AgNPs of concentration of 25 mg L^{-1} . Values represent mean \pm SD of three to five independent experiments. Different letters indicate significant differences ($p \leq 0.05$) between the tested systems in compared to controls

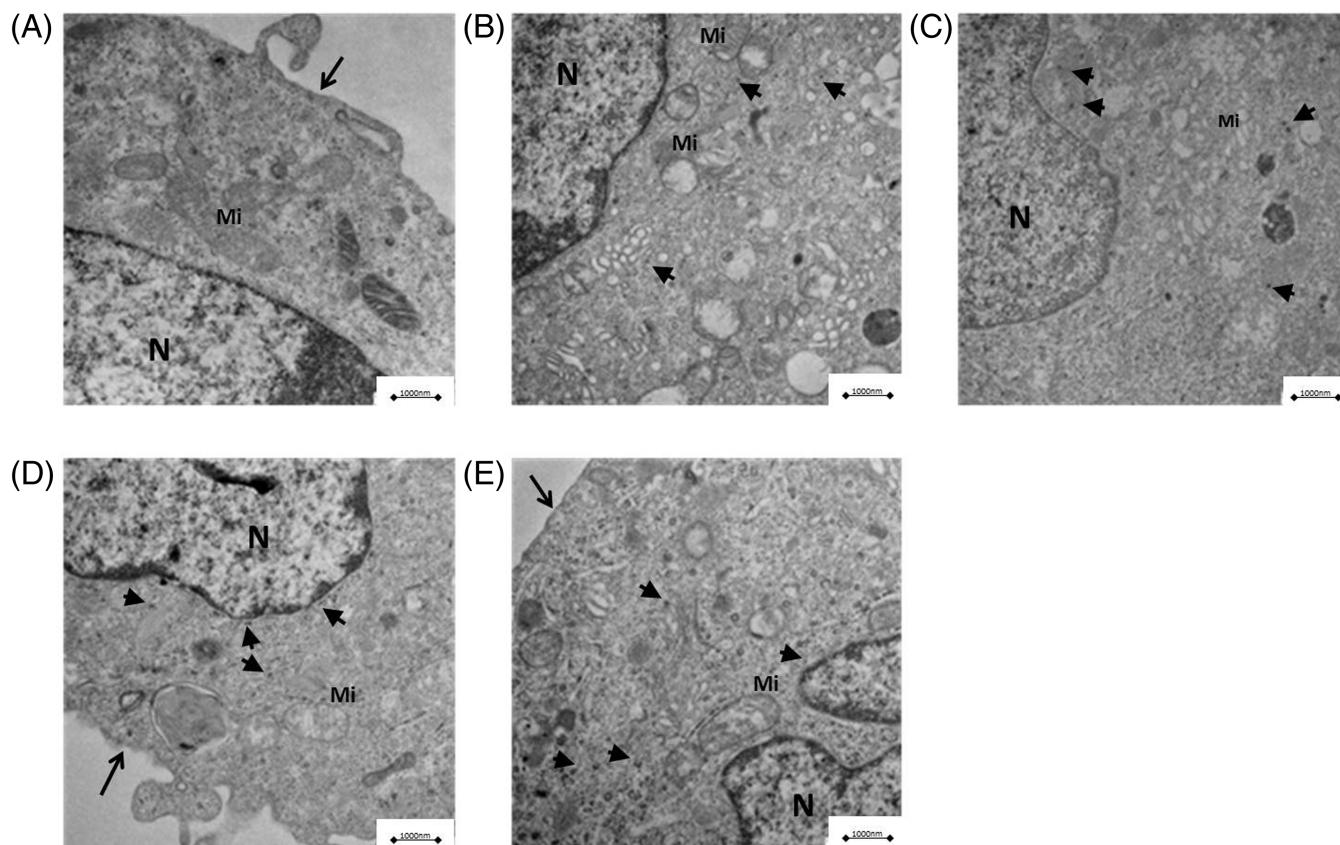


FIGURE 5 TEM micrographs of B16-F0 cells (A) before and after the 24-h exposure to (B) CAFGAAgNPs, (C) EGCGAgNPs, (D) EGCGGAAgNPs and (E) GAAgNPs of concentration of 25 mg L^{-1} . Open arrows show the membrane of cells whereas black thick arrows present AgNPs. Abbreviations: N—The cell nucleus, mi—Mitochondria. The scale bar show 1000 nm

membranes were observed in B16-F0 cells treated with CAFGAAgNPs. These AgNPs were present in the cytoplasm and in vesicular bodies (Figure 5B). Loosely dispersed AgNPs in the cytoplasm and numerous mitochondria without internal membranes were noticeable in the cells treated with EGCGAgNPs (Figure 5C). On the other hand, the cells treated with EGCGGAAgNPs showed a significant amount of fine active vesicles and possibly the AgNP binding to microtubules (Figure 5D). GAAgNPs-treated cells had numerous cytoplasmic vacuoles (Figure 5E).

4 | DISCUSSION

Effective treatment of malignant tumors is still in demand. Melanoma, derived from melanocytes, is one of the most highly invasive and metastatic tumors. A lot is known about the pathogenesis of melanoma: how the various signaling pathways work, why UV radiation is harmful, or what causes metastasis (Garbe & Leiter, 2009). For the research on the melanoma, two model cell lines were used to determine the impact of diverse AgNPs of comparable size distribution on them. The research involved two cell lines: mouse line B16-F0 and the human line COLO 679. It is worth mentioning that mouse B16-F0 cells are widely applied as model system for testing activity of anticancer drugs

(Kudugunti et al., 2011; Vad et al., 2014). Similarly, the utility of human COLO 679 cells was investigated as a skin tumor model (Vincent & Postovit, 2017). Nevertheless, to the best of our knowledge, the comparative studies on the impact of AgNPs on model mouse and human melanoma cell lines have not been carried out as so far.

Four types of negatively charged AgNPs of comparable size distribution and differentiated surface properties arising from the types of low molar mass antioxidants applied for their synthesis were in the center of this research interest. Numerous literature evidences documented that the biological activity of AgNPs are strongly correlated with their physicochemical properties. A crucial role is assigned to the impact of stabilizing agent molecules adsorbed on the AgNP surfaces, which tune surface charge and nanoparticle stability (Ferraris et al., 2017; Ravindran et al., 2013; Singh et al., 2010). The controlled surface modification of AgNPs is the latest research direction that can help to design and prepare colloidal systems of desired activity toward tumor cells. The stabilization of AgNPs by biologically active substances of confirmed anticancer activity seems to especially interesting in respect to potential application in medicine. It was well documented that diverse common antioxidants exhibiting anticancer activity can be useful stabilizers and reducing agents in the AgNP synthesis.

Essmann et al. (2004) showed that CAF, which can be a AgNP stabilizer, not only affects the cell cycle and growth arrest but also affects cancer cells via caspase-3 and p53 pathways. Lu et al. (2014) showed that CAF may have a cytotoxic effect on cancer cells by participating in the regulation of gene expression. EGCG has already been tested for antimelanoma activity (Ellis et al., 2011; Zhang et al., 2016). GA is recognized as having anticancer and anti-inflammatory properties (Locatelli et al., 2013). Therefore, it was hypothesized that the use of these antioxidants for the synthesis of AgNPs was to influence their bioactivity (Figure 6).

The insightful physicochemical characteristics of AgNPs prepared with the use of selected antioxidants revealed that they were characterized by spherical shape, comparable average size, and negative surface charge (Table 1). The AgNPs dispersed in aqueous suspensions were stable in broad range of pH and ionic strengths (Figures S5 and S6). Their stability was also confirmed in the cell culture media (Figures S2 and S3).

Based on the SERS spectra (Figures S7 and S8), it was established that negatively charged CAFGAAgNPs are mainly stabilized by unchanged molecules of CAF and GA, whereas in the stabilizing layers of GAAgNPs, oxidized forms of GA were detected. In the case of EGCGGAAgNPs and EGCGAgNPs, it was confirmed that EGCG molecules participate in the reaction of AgNP formation and at the surface of AgNPs probably occur in oxidized forms. EGCGGAAgNPs were stabilized by oxidized forms of EGCG and molecules of GA.

In order to evaluate the dependencies between the surface properties of AgNPs and their biological activity, the melanoma cells were exposed to pure antioxidant and the AgNPs of diverse concentrations over 24 h. Then, the biochemical and morphological changes in the treated cells were determined. It was found that the effect of the antioxidant itself on the cells was significantly different than the one induced by the antioxidant AgNPs.

Despite the fact that GA seemed to be the most toxic for the cells (Figure S9), any type of AgNPs obtained with its use was not the most destructive. EGCGAgNPs turned out to be the most destructive for the cells.

Detailed analysis of the toxicity of antioxidants at the concentration of value applied during the AgNP synthesis (EGCG 34 mg L⁻¹, CAF 156 mg L⁻¹, GA 25 mg L⁻¹) delivered significant information in respect to the toxicity of AgNPs. Because GA at concentration of 25 mg L⁻¹ and GAAgNPs at the highest investigated concentration decreased the cell viability to 60%–80% (Figure S9) and 70%–85% (Figure 1), one can conclude that any synergistic effects do not appear in this system. Based on the SERS analysis, one can explain that this effect mainly results from the oxidation of GA occurring during the AgNP synthesis. Because GAAgNPs were not stabilized only by pure GA molecules, the toxicity of oxidized forms of GA seems to be lower than GA molecules. The attention should be also paid on the fact that preparation of AgNPs with the use of mixtures of antioxidants influences their toxicity. CAFGAAgNPs and EGCGGAAgNPs applied at the highest concentration were more toxic for COLO 679 cells than GAAgNPs (Figure 1). It was established also that the selection of antioxidants used for the AgNP stabilization significantly influence on their toxicity in comparison with the model negatively charged AgNPs stabilized with citrate anions (Figure S10).

The selected antioxidants were also supposed to support the penetration of AgNPs into the cells, which was observed with the use of TEM. Chavva et al. (2019) demonstrated that EGCG-functionalized gold nanoparticles (AuNPs) were more effectively bound to the surface of melanoma cells compared with noncancerous cells, and these AuNPs induced melanoma cell apoptosis. Chen et al. (2014) showed that EGCG combined with AuNPs causes apoptosis via the mitochondrial pathway in B16-F10 melanoma cells. The viability studies performed during this research confirmed the highest cytotoxicity of

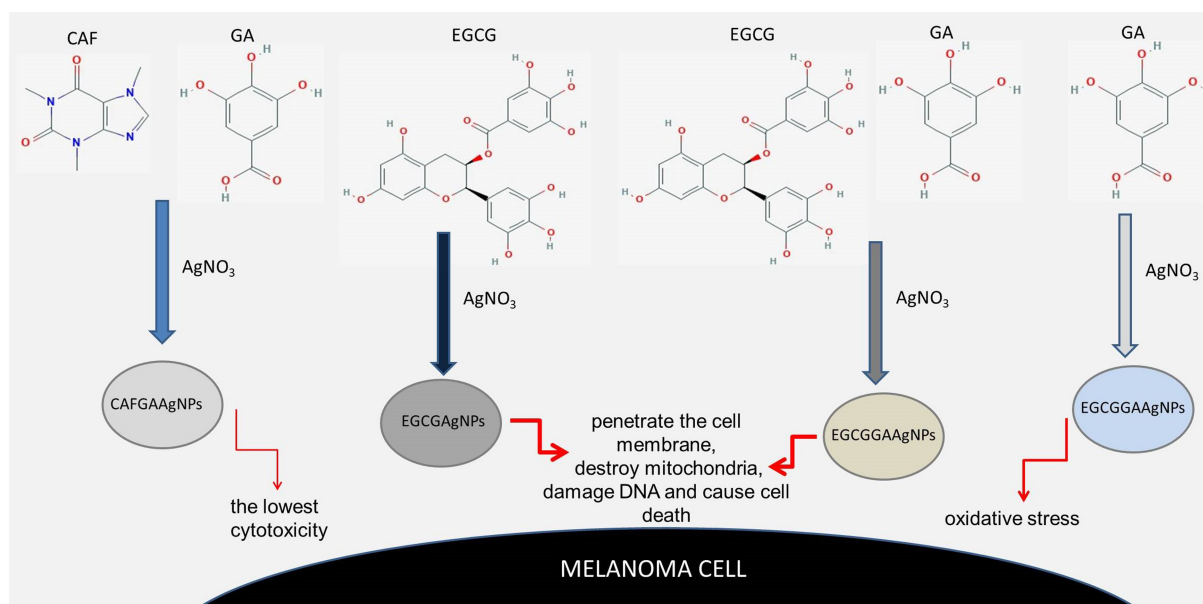


FIGURE 6 Scheme of bioactivity of AgNPs obtained with the use of selected low molecular mass antioxidants against melanoma cells

EGCGAgNPs against the melanoma cells. However, in comparison with a previous work, herein it was established that the AgNPs obtained with the use of EGCG are not stabilized by unreacted forms of this antioxidant. At the same time, a much greater sensitivity of the cells of the human line compared with cells of the mouse line was observed. This is especially visible in the determination of the cell membrane stability (LDH assay). Watanabe et al. (2012) showed that cell membrane stiffness is a key element of tumor metastasis. In their research, they used EGCG as a factor increasing cell membrane stiffness. However, it was EGCGAgNPs that caused the greatest leakage of LDH from inside the cells. It is worth mentioning that the presence of GA molecules at the surface of EGCGGAAgNPs noticeably decreased LDH release from the cells in comparison with the data obtained for EGCGAgNPs. Taking into account that both types of AgNPs were negatively charged and characterized by comparable values of zeta potential for a broad range of pH and ionic strength (Figure S6), one can state that the chemical structure of stabilizing layers of AgNPs plays a crucial role for their toxicity.

The result of exposure of cells to contact with the nanoparticles is their penetration into them. The uptake, translocation, and accumulation of AgNPs in cells depend on the cell structure, its membrane permeability, particle size, and other properties of the cell. Caballero-Díaz et al. (2013) linked the cytotoxicity and penetration capacity of AgNPs into cells with their surface chemistry. Kettler et al. (2016) has shown that uptake of silver nanoparticles by monocytic cells depends on particle size and presence of serum proteins. The tested nanoparticles penetrate the melanoma cells. However, the kinetics of this process and the quantitative measurement of AgNPs translocated inside the cells require further research.

It is worth paying attention to the comparison of data resulting from the incubation of antioxidants alone with cells or antioxidant-stabilized silver nanoparticles. The antioxidants themselves, as our research has shown, are not highly cytotoxic to the tested cell lines (even in the concentration of μg used for the synthesis of nanoparticles). They are less toxic than the silver nanoparticles produced with them. In turn, SBTCAgNPs are more toxic to the test cells than every antioxidant-stabilized silver nanoparticles. Nguyen et al. (2013) showed that uncoated AgNPs were more toxic than coated AgNPs (they used uncoated and PVP-coated silver nanoparticles for the study). Uncoated with AgNPs suppress inflammatory responses and enhance oxidative stress in test cells, whereas AgNP coated ones induce toxic effects by upregulating cytokines. The cell lines selected for the tests significantly differ in terms of their sensitivity to the tested substances. The obtained results indicate that the human COLO 679 cells are significantly more sensitive to the tested substances than the mouse cells.

Thus, the twice lower LDH leakage from B16-F0 in comparison with COLO 679 cells (Figure 2) seems to be directly related to the composition and physicochemical properties of their cell membranes. Analysis of the induction of inflammation (NO assay) showed that CAF and EGCG, known as anti-inflammatory agents (Bruce et al., 2002; Punathil et al., 2008), in combination with AgNPs exerted the strongest proinflammatory effects. In the case of EGCGAgNPs,

one can speculate that the oxidation of EGCG present in the nanoparticle stabilizing layer is a reason for lower anti-inflammatory properties in comparison with results obtained for other AgNPs.

However, the role of NO in promoting cancer formation is very complex. Yarlagadda et al. (2017) showed that NO can promote melanoma proliferation and inhibit apoptosis. Many *in vitro* studies have revealed that AgNPs interfere with the normal functioning of the cell, mainly as a result of the induction of oxidative stress. The toxicity of AgNPs is related to generation intracellular ROS, glutathione depletion (GSH), increase of lipid peroxidation in cells, and a reduction in the activity of the enzyme superoxide dismutase (SOD) (Arora et al., 2008; Barbasz, Oćwieja, & Walas, 2017; Hussain et al., 2005). Additionally, AgNP-induced oxidative stress is believed to be independent of the toxicity of silver ions generated inside cells during oxidative dissolution of AgNPs (Kim et al., 2009). Each type of the AgNPs tested in these studies exhibited negligible sensitivity to oxidative dissolution under tested external conditions. Each type of AgNPs increased the amount of ROS in samples. However, the highest relative amount of ROS was found after the cell treatment with GAAgNPs. This was reflected in the highest level of MDA after the treatment of GAAgNPs cells. The mechanisms of AgNPs toxicity related to the overproduction of ROS, which exceeds the capacity of antioxidant defense of cells, are based on the disruption of the main cell components (Lovrić et al., 2005; Xia et al., 2006). The enhanced production of MDA modifies the properties of cell membranes. Changes in asymmetry of membrane lipids, lower hydrophobicity, and depolarization of cells disrupt transport across the membrane and affect the interaction with the external environment of the cell. GAAgNPs was characterized by the highest cytotoxicity associated with the induction of oxidative stress, which may result from the chemistry of their stabilizing layer.

The TRO parameter provides information about the possible ways that cells “deal” with free radicals supplied from outside. The higher the TRO value expressed by the lower residual unreacted DPPH radical in the sample indicates, the greater the resistance of the system to oxidation. The highest TRO value was demonstrated for EGCG-combined AgNPs. Rudolphi-Skórska et al. (2018) showed that EGCG is more effective than GA in direct protection of the model cell membrane against oxidative stress. TEM imaging indicated that EGCGAgNPs and EGCGGAAgNPs had the highest cell penetration ability. They were even observed near the cell nucleus. The expansiveness of these AgNPs is also seen in the highest values of AP sites for both cell lines, as well as in perceived nuclear fragmentation in DAPI staining. AgNPs genotoxicity is associated with DNA damage, chromosomal aberrations, and cell cycle arrest (Asharani, Low Kah Mun, et al., 2009). The presence of EGCG in the stabilizing layer of AgNPs enhances also their toxicity.

The synthesis with the use of low molecular mass antioxidants results in a synergistic biological effect, which was demonstrated in studies on the bacteriostaticity of EGCGAgNPs (Durán et al., 2016). EGCG, as an antioxidant, effectively inhibits ROS activity inside cells (Skebo et al., 2007). Moulton et al. (2010) showed that nontoxic AgNPs can be obtained by using the “green synthesis” and the

cytotoxic effect of AgNPs can be eliminated by the addition of antioxidants (Braydich-Stolle et al., 2009). Our studies revealed that EGCG AgNPs induced a high ROS production that probably results from the oxidation forms of EGCGAgNPs present on the AgNP surface. It is worth mentioning that EGCGAgNPs did not induce such a high ROS production in comparison with GAAgNPs. Hence, one can conclude that the presence of diverse types of antioxidants or their oxidized forms tune cytotoxicity of whole nanometric system.

Green synthesis with the use of various plants leads to the formation of AgNPs embedded in their surface with numerous biological active compounds (Kumar et al., 2010). Synthesis using EGCG and GA did not enhance the cytotoxicity of nanoparticles compared with EGCGAgNPs or GAAgNPs, which mainly arises with the structural changes of these molecules occurring during the AgNP synthesis.

EGCGGAAgNP and EGCGAgNPs induced the strongest mitochondrial changes. It is interesting that these AgNPs were also characterized by the most negative values of zeta potential (Figure S6). Although CAFGAAgNPs and GAAgNPs exhibited comparable values of zeta potential, they induced diverse effect. CAFGAAgNPs were strongly immunogenic, whereas GAAgNPs caused strong ROS production, similarly as EGCGAgNPs, which in turn stimulated the LDH release. These findings showed that in the case of negatively charged AgNPs, not their electrokinetic charge, but instead mainly their structure of stabilizing layers, plays a pivotal role in the induction of biological activity.

Great interest among researchers is focused on green synthesis of AgNPs. The coating agents bind to the surface of the nanoparticles and prevent aggregation of nanoparticles. This increases the solubility, and it can serve as a site for bioconjugation of nanoparticles with the desired molecules; it also has another important meaning. Numerous literature reports indicate that AgNPs synthesized by using plant extracts are more cytotoxic with respect to cancer cells than normal cells. AlSalhi et al. (2019) showed that AgNPs obtained by green synthesis using palm dates show a potent antitumor activity against the MCF7 breast cancer cell line compared with the normal human mammary epithelial cell line MCF10A. Barua et al. (2016) showed that the cytotoxicity of Thuja extracted AgNPs was significantly higher in cancer cells compared with other normal cells. Also, Gurunathan et al. (2015) showed that the cancer cells showed a dose-dependent increase in cell death, whereas in normal cells, there was no significant lung cell toxic effect. An excellent list of literature data on this subject was prepared by Bhowmik et al. (2019). The use of natural antioxidants can support the anticancer effect of AgNPs. Although the issue of the effect on normal human cells requires further research, the current reports indicate that the use of natural antioxidants differentiates the action of AgNPs in relation to neoplastic and non-neoplastic cells.

Summarizing, it can be concluded that AgNPs synthesized with the use of EGCG were the most cytotoxic for the melanoma cells. EGCGAgNPs easily penetrated the cell membrane, destroyed mitochondria, damaged the DNA, and caused the cell death. The cytotoxicity of GAAgNPs was correlated with a high oxidative stress in the cells (increased lipid peroxidation and ROS in cells). CAFGAAgNPs showed the lowest cytotoxicity in relation to the melanoma cells

tested. Using a range of physicochemical and biochemical methods, we determined of the mechanism of action of AgNPs obtained with the use of selected antioxidants against the melanoma cells. Giving AgNPs specific properties may result in their preferential catching by neoplastic cells, and thus, they may become part of a targeted anti-cancer therapy.

ACKNOWLEDGMENTS

This work received financial support from the National Science Centre, Poland grant number DEC- 2019/03/X/NZ1/00305 - MINIATURA 3. We would like to thank Olga Woźnicka PhD from the Institute of Zoology, Jagiellonian University in Krakow, for her help with TEM imaging. The research was partially performed at the Institute of Nuclear Physics Polish Academy of Sciences using equipment purchased as part of a the project co-funded by the Malopolska Regional Operational Programme Measure 5.1 Krakow Metropolitan Area as an important hub of the European Research Area for 2007–2013, project No. MRPO.05.01.00-12-013/15oćwieja.

CONFLICT OF INTEREST

The authors declare that there is no conflict of interest.

DATA AVAILABILITY STATEMENT

The data that support the findings of this study are available from the corresponding author upon reasonable request.

ORCID

Anna Barbasz  <https://orcid.org/0000-0001-5210-2349>

Agnieszka Czyżowska  <https://orcid.org/0000-0003-3398-4475>

Natalia Piergies  <https://orcid.org/0000-0003-4899-3534>

Magdalena Oówieja  <https://orcid.org/0000-0002-7976-135X>

REFERENCES

- Ahmad, S., Hameed, A., Khan, K., Tauseef, I., Ali, M., Sultan, F., & Shahzad, M. (2019). Evaluation of synergistic effect of nanoparticles with antibiotics against enteric pathogens. *Applied Nanoscience*, 10, 3337–3340. <https://doi.org/10.1007/s13204-019-01201-3>
- AlSalhi, M. S., Elangovan, K., Ranjitsingh, A. J. A., Murali, P., & Devanesan, S. (2019). Synthesis of silver nanoparticles using plant derived 4-N-methyl benzoic acid and evaluation of antimicrobial, antioxidant and antitumor activity. *Saudi Journal of Biological Sciences*, 26(5), 970–978. <https://doi.org/10.1016/j.sjbs.2019.04.001>
- Alvarez-Ros, M. C., Sánchez-Cortés, S., Francioso, O., & García-Ramos, J. V. (2001). Catalytic modification of gallic acid on a silver surface studied by surface-enhanced Raman spectroscopy. *Journal of Raman Spectroscopy*, 32(2), 143–145. <https://doi.org/10.1002/jrs.683>
- Alvarez-Ros, M. C., Sanchez-Cortes, S., Francioso, O., & Garcia-Ramos, J. V. (2003). Adsorption and chemical modification of gallic acid on silver nanoparticles studied by Raman spectroscopy: Effect of anions and cationic pesticide paraquat. *Canadian Journal of Analytical Sciences and Spectroscopy*, 48(2), 132–138.
- Arora, S., Jain, J., Rajwade, J. M., & Paknikar, K. M. (2008). Cellular responses induced by silver nanoparticles: In vitro studies. *Toxicology Letters*, 179(2), 93–100. <https://doi.org/10.1016/j.toxlet.2008.04.009>
- Asharani, P. V., Hande, M. P., & Valiyaveetil, S. (2009). Anti-proliferative activity of silver nanoparticles. *BMC Cell Biology*, 10(1), 1–14. <https://doi.org/10.1186/1471-2121-10-65>

- Asharani, P. V., Low Kah Mun, G., Hande, M. P., & Valiyaveetil, S. (2009). Cytotoxicity and genotoxicity of silver nanoparticles in human cells. *ACS Nano*, 3(2), 279–290. <https://doi.org/10.1021/nn800596w>
- Bae, E., Park, H. J., Yoon, J., Kim, Y., Choi, K., & Yi, J. (2011). Bacterial uptake of silver nanoparticles in the presence of humic acid and AgNO₃. *Korean Journal of Chemical Engineering*, 28(1), 267–271. <https://doi.org/10.1007/s11814-010-0351-z>
- Barbasz, A., Oćwieja, M., Piergies, N., Duraczyńska, D., & Nowak, A. (2021). Antioxidant-modulated cytotoxicity of silver nanoparticles. *Journal of Applied Toxicology*. <https://doi.org/10.1002/jat.4173>
- Barbasz, A., Oćwieja, M., & Roman, M. (2017). Toxicity of silver nanoparticles towards tumoral human cell lines U-937 and HL-60. *Colloids and Surfaces B: Biointerfaces*, 156(1), 397–404. <https://doi.org/10.1016/j.colsurfb.2017.05.027>
- Barbasz, A., Oćwieja, M., & Walas, S. (2017). Toxicological effects of three types of silver nanoparticles and their salt precursors acting on human U-937 and HL-60 cells. *Toxicology Mechanisms and Methods*, 27(1), 58–71. <https://doi.org/10.1080/15376516.2016.1251520>
- Barua, S., Banerjee, P. P., Sadhu, A., Sengupta, A., Chatterjee, S., Sarkar, S., Barman, S., Chattopadhyay, A., Bhattacharya, S., Mondal, N. C., & Karak, N. (2016). Silver nanoparticle as antibacterial and anticancer materials against human breast, cervical and oral cancer cells. *Journal of Nanoscience and Nanotechnology*, 16, 1–9. <https://doi.org/10.1166/jnn.2016.12636>
- Bhowmik, A. D., Bandyopadhyay, A., & Chattopadhyay, A. (2019). Cytotoxic and mutagenic effects of green silver nanoparticles in cancer and normal cells: A brief review. *The Nucleus*, 62(3), 277–285. <https://doi.org/10.1007/s13237-019-00293-0>
- Blois, M. S. (1958). Antioxidant determinations by the use of a stable free radical. *Nature*, 181(4617), 1199–1200. <https://doi.org/10.1038/1811199a0>
- Bode, A. M., & Dong, Z. (2007). The enigmatic effects of caffeine in cell cycle and cancer. *Cancer Letters*, 247(1), 26–39. <https://doi.org/10.1016/j.canlet.2006.03.032>
- Braydich-Stolle, L. K., Schaeublin, N. M., Murdock, R. C., Jiang, J., Biswas, P., Schlager, J. J., & Hussain, S. M. (2009). Crystal structure mediates mode of cell death in TiO₂ nanotoxicity. *Journal of Nanoparticle Research*, 11(6), 1361–1374. <https://doi.org/10.1007/s11051-008-9523-8>
- Bruce, C., Yates, D. H., & Thomas, P. S. (2002). Caffeine decreases exhaled nitric oxide. *Thorax*, 57(4), 361–363. <https://doi.org/10.1136/thorax.57.4.361>
- Caballero-Díaz, E., Pfeiffer, C., Kastl, L., Rivera-Gil, P., Simonet, B., Valcárcel, M., Jiménez-Lamana, J., Laborda, F., & Parak, W. J. (2013). The toxicity of silver nanoparticles depends on their uptake by cells and thus on their surface chemistry. *Particle & Particle Systems Characterization*, 30(12), 1079–1085. <https://doi.org/10.1002/ppsc.201300215>
- Chavva, S. R., Deshmukh, S. K., Kanchanapally, R., Tyagi, N., Coym, J. W., Singh, A. P., & Singh, S. (2019). Epigallocatechin gallate-gold nanoparticles exhibit superior antitumor activity compared to conventional gold nanoparticles: Potential synergistic interactions. *Nanomaterials*, 9(3), 396. <https://doi.org/10.3390/nano9030396>
- Chen, C. C., Hsieh, D. S., Huang, K. J., Chan, Y. L., Hong, P. D., Yeh, M. K., & Wu, C. J. (2014). Improving anticancer efficacy of (–)-epigallocatechin-3-gallate gold nanoparticles in murine B16F10 melanoma cells. *Drug Design, Development and Therapy*, 8, 459. <https://doi.org/10.2147/DDDT.S58414>
- Chen, X., Gu, H., Shen, G., Dong, X., & Kang, J. (2010). Spectroscopic study of surface enhanced Raman scattering of caffeine on borohydride-reduced silver colloids. *Journal of Molecular Structure*, 975(1–3), 63–68. <https://doi.org/10.1016/j.molstruc.2010.03.085>
- Durán, N., Durán, M., De Jesus, M. B., Seabra, A. B., Fávaro, W. J., & Nakazato, G. (2016). Silver nanoparticles: A new view on mechanistic aspects on antimicrobial activity. *Nanomedicine: Nanotechnology, Biology and Medicine*, 12(3), 789–799. <https://doi.org/10.1016/j.nano.2015.11.016>
- El Badawy, A. M., Silva, R. G., Morris, B., Scheckel, K. G., Suidan, M. T., & Tolaymat, T. M. (2011). Surface charge-dependent toxicity of silver nanoparticles. *Environmental Science & Technology*, 45(1), 283–287. <https://doi.org/10.1021/es1034188>
- El-Hussein, A., Mfouo-Tynga, I., Abdel-Harith, M., & Abrahamse, H. (2015). Comparative study between the photodynamic ability of gold and silver nanoparticles in mediating cell death in breast and lung cancer cell lines. *Journal of Photochemistry and Photobiology B: Biology*, 153, 67–75. <https://doi.org/10.1016/j.jphotobiol.2015.08.028>
- Ellis, L. Z., Liu, W., Luo, Y., Okamoto, M., Qu, D., Dunn, J. H., & Fujita, M. (2011). Green tea polyphenol epigallocatechin-3-gallate suppresses melanoma growth by inhibiting inflammasome and IL-1 β secretion. *Biochemical and Biophysical Research Communications*, 414(3), 551–556. <https://doi.org/10.1016/j.bbrc.2011.09.115>
- Essmann, F., Engels, I. H., Totzke, G., Schulze-Osthoff, K., & Jänicke, R. U. (2004). Apoptosis resistance of MCF-7 breast carcinoma cells to ionizing radiation is independent of p53 and cell cycle control but caused by the lack of caspase-3 and a caffeine-inhibitable event. *Cancer Research*, 64(19), 7065–7072. <https://doi.org/10.1158/0008-5472.CAN-04-1082>
- Fayaz, A. M., Balaji, K., Girilal, M., Yadav, R., Kalaichelvan, P. T., & Venketesan, R. (2010). Biogenic synthesis of silver nanoparticles and their synergistic effect with antibiotics: A study against gram-positive and gram-negative bacteria. *Nanomedicine*, 6, 103–109. <https://doi.org/10.1016/j.nano.2009.04.006>
- Ferraris, S., Miola, M., Cochis, A., Azzimonti, B., Rimondini, L., Prenesti, E., & Vernè, E. (2017). In situ reduction of antibacterial silver ions to metallic silver nanoparticles on bioactive glasses functionalized with polyphenols. *Applied Surface Science*, 396, 461–470. <https://doi.org/10.1016/j.apsusc.2016.10.177>
- Garbe, C., & Leiter, U. (2009). Melanoma epidemiology and trends. *Clinics in Dermatology*, 27(1), 3–9. <https://doi.org/10.1016/j.clindermatol.2008.09.001>
- Garrido, C., Diaz-Fleming, G., & Campos-Vallette, M. M. (2016). SERS spectrum of gallic acid obtained from a modified silver colloid. *Spectrochimica Acta Part a: Molecular and Biomolecular Spectroscopy*, 163, 68–72. <https://doi.org/10.1016/j.saa.2016.03.028>
- Gichner, T. (1987). Two types of antimutagenic effects of gallic and tannic acids towards N-nitroso-compounds-induced mutagenicity in the Ames Salmonella assay. *Folia Microbiologica*, 32, 55–62. <https://doi.org/10.1007/BF02877259>
- Gorczyca, A., Pocięcha, E., Kasprzowicz, M., & Niemiec, M. (2015). Effect of nanosilver in wheat seedlings and *Fusarium culmorum* culture systems. *European Journal of Plant Pathology*, 142(2), 251–261. <https://doi.org/10.1007/s10658-015-0608-9>
- Gurunathan, S., Jeong, J. K., Han, J. W., Zhang, X. F., Park, J. H., & Kim, J. H. (2015). Multidimensional effects of biologically synthesized silver nanoparticles in *helicobacter pylori*, *helicobacter felis*, and human lung (L132) and lung carcinoma A549 cells. *Nanoscale Research Letters*, 10(1), 1–17. <https://doi.org/10.1186/s11671-015-0747-0>
- He, Y., Du, Z., Ma, S., Cheng, S., Jiang, S., Liu, Y., Li, D., Huang, H., Zhang, K., & Zheng, X. (2016). Biosynthesis, antibacterial activity and anticancer effects against prostate cancer (PC-3) cells of silver nanoparticles using *Dimocarpus Longan Lour.* Peel extract. *Nanoscale Research Letters*, 11(1), 1–10. <https://doi.org/10.1186/s11671-016-1511-9>
- Hong, J., Lu, H., Meng, X., Ryu, J. H., Hara, Y., & Yang, C. S. (2002). Stability, cellular uptake, biotransformation, and efflux of tea polyphenol (–)-epigallocatechin-3-gallate in HT-29 human colon adenocarcinoma cells. *Cancer Research*, 62(24), 7241–7246.
- Huang, C. C., & Chen, W. (2018). A SERS method with attomolar sensitivity: A case study with the flavonoid catechin. *Microchimica Acta*, 185(2), 120. <https://doi.org/10.1007/s00604-017-2662-9>

- Hussain, S. M., Hess, K. L., Gearhart, J. M., Geiss, K. T., & Schlager, J. J. (2005). In vitro toxicity of nanoparticles in BRL 3A rat liver cells. *Toxicology in Vitro*, 19(7), 975–983. <https://doi.org/10.1016/j.tiv.2005.06.034>
- Hwang, I. S., Hwang, J. H., Choi, H., Kim, K. J., & Lee, D. G. (2012). Synergistic effects between silver nanoparticles and antibiotics and the mechanisms involved. *Journal of Medical Microbiology*, 61(12), 1719–1726. <https://doi.org/10.1099/jmm.0.047100-0>
- Inoue, M., Suzuki, R., Sakaguchi, N., Li, Z., Takeda, T., Ogihara, Y., Jiang, B., & Chen, Y. (1995). Selective induction of cell death in cancer cells by gallic acid. *Biological & Pharmaceutical Bulletin*, 18, 1526–1530. <https://doi.org/10.1248/bpb.18.1526>
- Kang, J., Gu, H., Zhong, L., Hu, Y., & Liu, F. (2011). The pH dependent Raman spectroscopic study of caffeine. *Spectrochimica Acta Part a: Molecular and Biomolecular Spectroscopy*, 78(2), 757–762. <https://doi.org/10.1016/j.saa.2010.11.055>
- Kettler, K., Giannakou, C., de Jong, W. H., Hendriks, A. J., & Krystek, P. (2016). Uptake of silver nanoparticles by monocytic THP-1 cells depends on particle size and presence of serum proteins. *Journal of Nanoparticle Research*, 18(9), 1–9. <https://doi.org/10.1007/s11051-016-3595-7>
- Kim, D. O., Lee, K. W., Lee, H. J., & Lee, C. Y. (2002). Vitamin C equivalent antioxidant capacity of phenolic phytochemicals. *Journal of Agricultural and Food Chemistry*, 50, 3713–3717. <https://doi.org/10.1021/jf020071c>
- Kim, S., Choi, J. E., Choi, J., Chung, K. H., Park, K., Yi, J., & Ryu, D. Y. (2009). Oxidative stress-dependent toxicity of silver nanoparticles in human hepatoma cells. *Toxicology in Vitro*, 23(6), 1076–1084. <https://doi.org/10.1016/j.tiv.2009.06.001>
- Kittler, S., Greulich, C., Diendorf, J., Koller, M., & Epple, M. (2010). Toxicity of silver nanoparticles increases during storage because of slow dissolution under release of silver ions. *Chemistry of Materials*, 22(16), 4548–4554. <https://doi.org/10.1021/cm100023p>
- Kroes, B. H., van den Berg, A. J. J., Quarles van Ufford, H. C., van Dijk, H., & Labadie, R. P. (1992). Anti-inflammatory activity of gallic acid. *Planta Medica*, 58, 499–504. <https://doi.org/10.1055/s-2006-961535>
- Kudugunti, S. K., Vad, N. M., Ekogbo, E., & Moridani, M. Y. (2011). Efficacy of caffeic acid phenethyl ester (CAPE) in skin B16-F0 melanoma tumor bearing C57BL/6 mice. *Investigational New Drugs*, 29(1), 52–62. <https://doi.org/10.1007/s10637-009-9334-5>
- Kujda, M., Oćwieja, M., Adamczyk, Z., Bocheńska, O., Braś, G., Kozik, A., Bielańska, E., & Barbasz, J. (2015). Charge stabilized silver nanoparticles applied as antibacterial agents. *Journal of Nanoscience and Nanotechnology*, 15(5), 3574–3583. <https://doi.org/10.1166/jnn.2015.9727>
- Kumar, V., Yadav, S. C., & Yadav, S. K. (2010). Syzygiumcumini leaf and seed extract mediated biosynthesis of silver nanoparticles and their characterization. *Journal of Chemical Technology & Biotechnology*, 85(10), 1301–1309. <https://doi.org/10.1002/jctb.2427>
- Kumar-Krishnan, S., Prokhorov, E., Hernández-Iturriaga, M., Mota-Morales, J. D., Vázquez-Lepe, M., Kovalenko, Y., & Luna-Bárceñas, G. (2015). Chitosan/silver nanocomposites: Synergistic antibacterial action of silver nanoparticles and silver ions. *European Polymer Journal*, 67, 242–251. <https://doi.org/10.1016/j.eurpolymj.2015.03.066>
- Lara, H. H., Ixtapan-Turrent, L., Garza-Treviño, E. N., & Rodríguez-Padilla, C. (2010). PVP-coated silver nanoparticles block the transmission of cell-free and cell-associated HIV-1 in human cervical culture. *Journal of Nanobiotechnology*, 8(1), 1–11. <https://doi.org/10.1186/1477-3155-8-15>
- Lee, S. H., & Jun, B. H. (2019). Silver nanoparticles: Synthesis and application for nanomedicine. *International Journal of Molecular Sciences*, 20(4), 865. <https://doi.org/10.3390/ijms20040865>
- Locatelli, C., Filippin-Monteiro, F. B., & Creczynski-Pasa, T. B. (2013). Alkyl esters of gallic acid as anticancer agents: A review. *European Journal of Medicinal Chemistry*, 60, 233–239. <https://doi.org/10.1016/j.ejmech.2012.10.056>
- Lovrić, J., Cho, S. J., Winnik, F. M., & Maysinger, D. (2005). Unmodified cadmium telluride quantum dots induce reactive oxygen species formation leading to multiple organelle damage and cell death. *Chemistry & Biology*, 12(11), 1227–1234. <https://doi.org/10.1016/j.chembiol.2005.09.008>
- Lu, G. Y., Huang, S. M., Liu, S. T., Liu, P. Y., Chou, W. Y., & Lin, W. S. (2014). Caffeine induces tumor cytotoxicity via the regulation of alternative splicing in subsets of cancer-associated genes. *The International Journal of Biochemistry & Cell Biology*, 47, 83–92. <https://doi.org/10.1016/j.biocel.2013.12.004>
- Lu, L., Sun, R. W., Chen, R., Hui, C. K., Ho, C. M., Luk, J. M., Lau, G. K., & Che, C. M. (2008). Silver nanoparticles inhibit hepatitis B virus replication. *Antiviral Therapy*, 13(2), 253–262.
- Moulton, M. C., Braydich-Stolle, L. K., Nadagouda, M. N., Kunzleman, S., Hussain, S. M., & Varma, R. S. (2010). Synthesis, characterization and biocompatibility of “green” synthesized silver nanoparticles using tea polyphenols. *Nanoscale*, 2(5), 763–770. <https://doi.org/10.1039/CONR00046A>
- Nguyen, K. C., Seligy, V. L., Massarsky, A., Moon, T. W., Rippstein, P., Tan, J., & Tayabali, A. F. (2013, April). Comparison of toxicity of uncoated and coated silver nanoparticles. *Journal of Physics: Conference Series*, 429, 012025. <https://doi.org/10.1088/1742-6596/429/1/012025>
- Oćwieja, M., & Adamczyk, Z. (2014). Monolayers of silver nanoparticles obtained by chemical reduction methods. *Surface Innovations*, 2(3), 160–172. <https://doi.org/10.1680/si.13.00042>
- Oćwieja, M., & Barbasz, A. (2020). Sodium hexametaphosphate-induced enhancement of silver nanoparticle toxicity towards leukemia cells. *Journal of Nanoparticle Research*, 22(6), 1–16. <https://doi.org/10.1007/s11051-020-04903-w>
- Oćwieja, M., Barbasz, A., Walsa, S., Roman, M., & Paluszkiwicz, C. (2017). Physicochemical properties and cytotoxicity of cysteine-functionalized silver nanoparticles. *Colloids and Surfaces B: Biointerfaces*, 160(1), 429–437. <https://doi.org/10.1016/j.colsurfb.2017.09.042>
- Panáček, A., Kolár, M., Vecerová, R., Pucek, R., Soukupová, J., Krystof, V., Hamal, P., Zboril, R., & Kvítek, L. (2009). Antifungal activity of silver nanoparticles against *Candida* spp. *Biomaterials*, 30(31), 6333–6340. <https://doi.org/10.1016/j.biomaterials.2009.07.065>
- Pavel, I., Szeghalmi, A., Moigno, D., Cintă, S., & Kiefer, W. (2003). Theoretical and pH dependent surface enhanced Raman spectroscopy study on caffeine. *Biopolymers: Original Research on Biomolecules*, 72(1), 25–37. <https://doi.org/10.1002/bip.10248>
- Peter, B., Saftics, A., Kovacs, B., Kurunczi, S., & Horvath, R. (2020). Oxidation increases the binding of EGCG to serum albumin revealed by kinetic data from label-free optical biosensor with reference channel. *Analyst*, 145(2), 588–595. <https://doi.org/10.1039/c9an01779h>
- Pilaquinga, F., Morey, J., Torres, M., Seqqat, R., & Pina, M. D. L. N. (2021). Silver nanoparticles as a potential treatment against SARS-CoV-2: A review (Vol. 13) (e1707). *Nanomedicine and Nanobiotechnology*. <https://doi.org/10.1002/wnan.1707>
- Punathil, T., Tollefsbol, T. O., & Katiyar, S. K. (2008). EGCG inhibits mammary cancer cell migration through inhibition of nitric oxide synthase and guanylate cyclase. *Biochemical and Biophysical Research Communications*, 375(1), 162–167. <https://doi.org/10.1016/j.bbrc.2008.07.157>
- Qin, Y., Ji, X., Jing, J., Liu, H., Wu, H., & Yang, W. (2010). Size control over spherical silver nanoparticles by ascorbic acid reduction. *Colloids and Surfaces a: Physicochemical and Engineering Aspects*, 372(1–3), 172–176. <https://doi.org/10.1016/j.colsurfa.2010.10.013>
- Ravindran, A., Chandran, P., & Khan, S. S. (2013). Biofunctionalized silver nanoparticles: Advances and prospects. *Colloids and Surfaces B: Biointerfaces*, 105, 342–352. <https://doi.org/10.1016/j.colsurfb.2012.07.036>

- Ruden, S., Hilpert, K., Berditsch, M., Wadhvani, P., & Ulrich, A. S. (2009). Synergistic interaction between silver nanoparticles and membrane-permeabilizing antimicrobial peptides. *Antimicrobial Agents and Chemotherapy*, 53, 3538–3540. <https://doi.org/10.1128/AAC.01106-08>
- Rudolphi-Skórska, E., Dyba, B., Kreczmer, B., & Filek, M. (2018). Impact of polyphenol-rich green tea extracts on the protection of DOPC monolayer against damage caused by ozone induced lipid oxidation. *Acta Biochimica Polonica*, 65(2), 193–197. https://doi.org/10.18388/abp.2018_2612
- Singh, A. K., Talat, M., Singh, D. P., & Srivastava, O. N. (2010). Biosynthesis of gold and silver nanoparticles by natural precursor clove and their functionalization with amine group. *Journal of Nanoparticle Research*, 12(5), 1667–1675. <https://doi.org/10.1007/s11051-009-9835-3>
- Skebo, J. E., Grabinski, C. M., Schrand, A. M., Schlager, J. J., & Hussain, S. M. (2007). Assessment of metal nanoparticle agglomeration, uptake, and interaction using high-illuminating system. *International Journal of Toxicology*, 26(2), 135–141. <https://doi.org/10.1080/10915810701226248>
- Tanvir, F., Yaqub, A., Tanvir, S., & Anderson, W. A. (2017). Poly-L-arginine coated silver nanoprisms and their anti-bacterial properties. *Nanomaterials*, 7(10), 296. <https://doi.org/10.3390/nano7100296>
- Thawonsuwan, J., Kiron, V., Satoh, S., Panigrahi, A., & Verlhac, V. (2010). Epigallocatechin-3-gallate (EGCG) affects the antioxidant and immune defense of the rainbow trout, *Oncorhynchus mykiss*. *Fish Physiology and Biochemistry*, 36(3), 687–697. <https://doi.org/10.1007/s10695-009-9344-4>
- Vad, N. M., Kudugunti, S. K., Wang, H., Bhat, G. J., & Moridani, M. Y. (2014). Efficacy of acetylsalicylic acid (aspirin) in skin B16-F0 melanoma tumor-bearing C57BL/6 mice. *Tumor Biology*, 35(5), 4967–4976. <https://doi.org/10.1007/s13277-014-1654-1>
- Vincent, K. M., & Postovit, L. M. (2017). Investigating the utility of human melanoma cell lines as tumour models. *Oncotarget*, 8(6), 10498. <https://doi.org/10.18632/oncotarget.14443>
- Watanabe, T., Kuramochi, H., Takahashi, A., Imai, K., Katsuta, N., Nakayama, T., Fujiki, H., & Suganuma, M. (2012). Higher cell stiffness indicating lower metastatic potential in B16 melanoma cell variants and in (–)-epigallocatechin gallate-treated cells. *Journal of Cancer Research and Clinical Oncology*, 138(5), 859–866. <https://doi.org/10.1007/s00432-012-1159-5>
- Xia, J., Wang, D., Liang, P., Zhang, D., Du, X., Ni, D., & Yu, Z. (2020). Vibrational (FT-IR, Raman) analysis of tea catechins based on both theoretical calculations and experiments. *Biophysical Chemistry*, 256, 106282. <https://doi.org/10.1016/j.bpc.2019.106282>
- Xia, T., Kovochich, M., Brant, J., Hotze, M., Sempf, J., Oberley, T., Sioutas, C., Yeh, J. I., Wiesner, M. R., & Nel, A. E. (2006). Comparison of the abilities of ambient and manufactured nanoparticles to induce cellular toxicity according to an oxidative stress paradigm. *Nano Letters*, 6(8), 1794–1807. <https://doi.org/10.1021/nl061025k>
- Yarlagadda, K., Hassani, J., Foote, I. P., & Markowitz, J. (2017). The role of nitric oxide in melanoma. *Biochimica et Biophysica Acta (BBA)-Reviews on Cancer*, 1868(2), 500–509. <https://doi.org/10.1016/j.bbcan.2017.09.005>
- Zbinden, G., & Flury-Roversi, M. (1981). Significance of the LD 50-test for the toxicological evaluation of chemical substances. *Archives of Toxicology*, 47(2), 77–99. <https://doi.org/10.1007/BF00332351>
- Zhang, J., Lei, Z., Huang, Z., Zhang, X., Zhou, Y., Luo, Z., Zeng, W., Su, J., Peng, C., & Chen, X. (2016). Epigallocatechin-3-gallate (EGCG) suppresses melanoma cell growth and metastasis by targeting TRAF6 activity. *Oncotarget*, 7(48), 79557–79571. <https://doi.org/10.18632/oncotarget.12836>
- Zhu, Y., Xu, J., Wang, Y., Chen, C., Gu, H., Chai, Y., & Wang, Y. (2020). Silver nanoparticles-decorated and mesoporous silica coated single-walled carbon nanotubes with an enhanced antibacterial activity for killing drug-resistant bacteria. *Nano Research*, 13, 389–400. <https://doi.org/10.1007/s12274-020-2621-3>

SUPPORTING INFORMATION

Additional supporting information may be found in the online version of the article at the publisher's website.

How to cite this article: Barbasz, A., Czyżowska, A., Piergies, N., & Oćwieja, M. (2022). Design cytotoxicity: The effect of silver nanoparticles stabilized by selected antioxidants on melanoma cells. *Journal of Applied Toxicology*, 42(4), 570–587. <https://doi.org/10.1002/jat.4240>